Type IV-A3 CRISPR-Cas systems drive inter-plasmid conflicts by acquiring spacers in trans

Fabienne Benz, Sarah Camara-Wilpert, Jakob Russel, Katharina Wandera, Rimvydė Čepaitė, Manuel Ares-Arroyo, José Vicente Gomes-Filho, Frank Englert, Johannes Kuehn, Silvana Gloor, et al.

Type IV-A3 CRISPR-Cas systems drive inter-plasmid conflicts by acquiring spacers *in trans*

*Fabienne Benz[1-4,†], Sarah Camara-Wilpert[3,†], Jakob Russel[3], Katharina G. Wandera[5], Rimvydė Čepaitė[6], Manuel Ares-Arroyo[2], José Vicente Gomes Filho[7], Frank Englert[5], Johannes Kuehn[3], Silvana Gloor[4], Mario Rodríguez Mestre[3], Aline Cuénod[8, 9,10], Mònica Aguilà-Sans[3], Lorrie Maccario[3], Adrian Egli[8, 9,11], Lennart Randau[7,12], Patrick Pausch[6], Eduardo P. C. Rocha[2], Chase L. Beisel[5,13], Jonas Stenløkke Madsen[3], David Bikard[1], Alex R. Hall[4], Søren Johannes Sørensen[3,**], Rafael Pinilla-Redondo[3,*]*

[1] Institut Pasteur, Université Paris Cité, CNRS UMR6047, 75015 Paris, Synthetic Biology, Paris 75015, France
[2] Institut Pasteur, Université Paris Cité, CNRS UMR3525,Microbial Evolutionary Genomics Paris 75015, France
[3] Section of Microbiology, University of Copenhagen, Universitetsparken 15, 2100 Copenhagen, Denmark
[4] Institute of Integrative Biology, Department of Environmental Systems Science, ETH Zurich, Zurich, Switzerland
[5] Helmholtz Institute for RNA-based Infection Research (HIRI), Helmholtz Centre for Infection Research (HZI), Würzburg, Germany
[6] Life Sciences Center - European Molecular Biology Laboratory (LSC-EMBL) Partnership for Genome Editing Technologies, Vilnius University - Life Sciences Center, Vilnius University, Vilnius 10257, Lithuania
[7] Department of Biology, Philipps Universität Marburg, Marburg, Germany
[8] Applied Microbiology Research, Department of Biomedicine, University of Basel, Basel, Switzerland
[9] Division of Clinical Bacteriology and Mycology, University Hospital Basel, Basel, Switzerland
[10] Department of Microbiology and Immunology, McGill University, Montreal, QC, Canada
[11] Institute of Medical Microbiology, University of Zurich, Zürich, Switzerland
[12] SYNMIKRO, Center for Synthetic Microbiology, Marburg, Germany
[13] Medical Faculty, University of Würzburg, Würzburg, Germany

[†]*Joint first authors*

* Lead contact footnote:
Name: Rafael Pinilla-Redondo
E-mail: rafael.pinilla@bio.ku.dk

**Co-corresponding email addresses:
sjs@bio.ku.dk
rafael.pinilla@bio.ku.dk

Summary

Plasmid-encoded type IV-A CRISPR-Cas systems lack an acquisition module, feature a DinG helicase instead of a nuclease, and form ribonucleoprotein complexes. Type IV-A3 systems are carried by conjugative plasmids that often harbor antibiotic resistance genes. Their CRISPR array contents suggest a role in inter-plasmid conflicts, but this function remains unexplored. Here, we demonstrate that a plasmid-encoded type IV-A3 system co-opts the type I-E adaptation machinery from its host, *Klebsiella pneumoniae*, to update its CRISPR array. Furthermore, we reveal that robust interference of conjugative plasmids and phages is elicited through CRISPR RNA-dependent transcriptional repression. By silencing plasmid core functions, type IV-A3 impacts the horizontal transfer and stability of targeted plasmids, supporting its role in plasmid competition. Our findings shed light on the mechanisms and ecological function of type IV-A3 systems and demonstrate their practical efficacy for countering antibiotic resistance in clinically relevant strains.

Introduction

CRISPR-Cas systems protect bacteria from invading mobile genetic elements (MGEs) by providing adaptive immunity. Essential to their memory acquisition is the conserved Cas1-Cas2 adaptation module, which excises short sequences (protospacers) adjacent to a motif (PAM) in invading MGEs and incorporates them into the CRISPR array as new spacers (**Figure 1A**). Array transcription is followed by processing into mature CRISPR RNAs (crRNAs), which assemble with Cas proteins into crRNA-guided effector complexes that target and disrupt complementary sequences, typically through nuclease cleavage [1,2].

Type IV CRISPR-Cas systems have remained largely understudied, in contrast to most other known CRISPR-Cas types [3]. Like other Class 1 systems [4], they form multiprotein complexes [5–7] and are divided into distinct subtypes (IV-A to E) and variants (IV-A1 to 3), based on their molecular architecture [8,9]. Although type IV loci contain CRISPR arrays with varying spacer content, they typically lack Cas1-Cas2 adaptation modules, rendering their spacer acquisition mechanism enigmatic (**Figure 1A**) [8,10,11]. Type IV CRISPR-Cas systems also stand out for their consistent association with conjugative MGEs, such as plasmids and integrative conjugative elements (ICEs) [5,8,10,12], and in case of the type IV-A for featuring a 5'-3' DNA helicase called DinG instead of an effector nuclease (**Figure 1A**) [10,13].

Recent research has shed light on the potential mechanisms driving RNA-guided type IV CRISPR-Cas targeting. For example, the type IV-A CRISPR-Cas system (variant IV-A1) in *Pseudomonas oleovorans* has been shown to mediate DinG-dependent transcriptional repression of chromosomal targets [14]. Furthermore, type IV-A1 systems can facilitate the loss of a small vector plasmid even when the targeted region is outside an open reading frame [11,14], leaving open questions about the proposed CRISPR interference (CRISPRi) mechanism. Notably, type IV CRISPR arrays are enriched with spacers matching large conjugative plasmids, suggesting a unique role in inter-plasmid conflicts [8,10,12]. However, their ecological role and whether and how they can interfere with conjugative plasmids remain unexplored.

Here, through a combination of molecular genetics, bioinformatics, and biochemical analyses, we functionally characterize a type IV-A3 CRISPR-Cas system encoded on a *Klebsiella pneumoniae* conjugative plasmid. Our results reveal that type IV-A3 can acquire spacers by co-opting the host-derived type I-E adaptation machinery. Additionally, we show that crRNA-guided targeting can mediate the loss of conjugative plasmids through transcriptional repression of plasmid core functions and demonstrate that this silencing activity can be repurposed to re-sensitize bacteria to antibiotics. Because type IV-A3 systems are widespread among the pervasive and opportunistically pathogenic *K. pneumoniae* [8,12,15], our findings have important implications for understanding plasmid-driven adaptation, including prevention and dissemination of antibiotic resistance and virulence factors.

Results

A clinical *K. pneumoniae* conjugative plasmid encodes an active type IV-A3 CRISPR-Cas

Type IV-A3 systems are carried by large conjugative plasmids in *Enterobacteriaceae* (median size 280 kb), predominantly within the *Klebsiella* genus (91 %; **Figure S1A-D**) [8,12]. These plasmids are usually combinations of different replicons (cointegrates), most commonly IncHI1B/IncFIB (53%; **Figure S1E**), and frequently carry one or more antibiotic resistance genes (58%, on average 11 resistance genes/plasmid; **Figure S1F-H**) [15].

To investigate the biological function and molecular mechanisms driving adaptation and interference in type IV-A CRISPR-Cas, we aimed to establish a model system with ecological and clinical relevance. We selected the clinical isolate *K. pneumoniae* 808330 (sequence type ST182, capsular type KL47 and O-serotype OL101), which has a chromosomal type I-E CRISPR-Cas system and harbors plasmid p1530 that encodes a type IV-A3 CRISPR-Cas system (**Figure 1B-D, Figure S2, Table S1**). The IncHI1B/IncFIB p1530 is 205 kb and encodes the extended-spectrum β-lactamase (ESBL)-gene $bla_{CTX\text{-}M\text{-}15}$ that has spread globally and confers resistance to important 3rd generation cephalosporins [16,17]. Through conjugation experiments, we confirmed the ability of p1530 to transfer from its natural host into other clinical strains, including *Escherichia coli, K. pneumoniae,* and a *Salmonella enterica* Typhimurium (**Figure 1E**).

Our analysis of the CRISPR spacer contents in p1530 confirmed the strong preference for targeting other conjugative plasmids predicted across type IV CRISPR-Cas systems (**Fig 1F, Figure S2, Table S2**) [8]. Small RNA sequencing of *E. coli* expressing the type IV-A3 system from a plasmid showed the production of mature crRNAs (**Figure 1F, Figure S3A**). We then confirmed the constitutive expression and crRNA maturation of the type IV-A3 and type I-E CRISPR-Cas systems in their native *Klebsiella* host (**Figure S3B-C**). Finally, heterologous protein expression and purification revealed the formation of a ribonucleoprotein complex, containing the Cas proteins Cas8 (Csf1), Cas6 (Csf5), Cas5 (Csf3), and multiple Cas7 (Csf2), as well as nonstoichiometric copurified DinG (**Figure S3D-F**). This shows that the type IV-A3 Cas proteins assemble into a multisubunit complex and indicates that DinG may be recruited to the interference complex *in trans* after target binding (**Figure S3G**), similar to what has been observed for DinG in CRISPR-Cas type IV-A1 [7] and Cas3 in CRISPR-Cas type I [4]. These results collectively suggest that the *K. pneumoniae* type IV-A3 system in p1530 is both functional and suitable as a model system.

In trans use of Cas1/2e facilitates spacer acquisition in type IV-A3 CRISPR arrays

The overwhelming majority of type IV-A loci lack adaptation modules despite their association with CRISPR arrays with varying spacer content [8,18], prompting questions about the spacer acquisition mechanism (**Figure 1A**). Notably, type IV-A3 systems are frequently found in strains that encode chromosomal type I-E systems, and they share significant similarities in

their CRISPR repeats and leader sequence motifs, which are crucial for Cas1/2e-mediated spacer acquisition (**Figure S4A-B**) [8 19–22].

To investigate the potential functional interplay between type IV-A3 CRISPR arrays and type I-E adaptation modules, we expressed *K. pneumoniae* Cas1e and Cas2e (Cas1/2e) in *E. coli* harboring the type IV-A3-encoding plasmid p1530. To enhance rare spacer acquisition events, we electroporated cells with 35 bp double-stranded DNA oligos as protospacers (PS) containing the canonical type I-E 5'-AAG-3' spacer acquisition motif (SAM) (**Figure 2A, Figure S4C**) [23]. PCR analysis revealed Cas1/2e-dependent array expansion (**Figure 2B, Suppl. Fig S4D**), and Sanger sequencing confirmed integration of the electroporated protospacer into the leader-repeat junction of the type IV-A3 CRISPR array in p1530 (**Figure 2B)**. Notably, the 3'-guanine of the SAM is incorporated into the CRISPR array together with the spacer (**Figure 2B** bottom, **Suppl. Fig S5E**), which is a distinctive characteristic of type I-E adaptation [24–26].

To further characterize Cas1/2e-mediated spacer acquisition into type IV-A3 arrays and the corresponding SAM, we overexpressed Cas1/2e in *K. pneumoniae* 808330 harboring p1530 with a targeting-deficient type IV-A3 (Δ*dinG*) to allow for genome-wide spacer acquisition (**Figure 2A**). We PCR-amplified and deep-sequenced expanded CRISPR arrays (**Figure 2C, Figure S4F**) [27] and mapped the acquired spacers back to the *K. pneumoniae* 808330 genome. Consistent with the acquisition in I-E CRISPR-Cas systems, the majority of acquired spacers were 32 bp in length (85 %, n= 13M total; **Figure 2D**) and preferentially originated from genomic positions next to a 5'-AAG-3' SAM (positions -3 to -1, **Figure 2E**) [24–26]. Furthermore, we observed a preference for the acquisition of spacers from plasmids in the cell (**Figure S4G**), consistent with previous reports describing type I-E adaptation [28], and no preference for the coding and template strands (**Figure S4H**). Surprisingly, we did not observe spacer acquisition in the chromosomal type I-E array of *K. pneumoniae* 808330 under our experimental conditions. This was independent of presence or absence of the IV-A3 system in the cell **(Figure S4F**). Together, our findings demonstrate that plasmid-encoded type IV-A3 CRISPR-Cas systems can use host-derived Cas1/2e to acquire new spacers.

IV-A3 targeting interferes with horizontal transfer and stability of conjugative plasmids

Type IV-A3 CRISPR-Cas spacers exhibit a prominent bias towards targeting plasmids (86% of predicted targets; **Figure S5A)**, especially those that are large and conjugative (median size 136 kb, 67 % conjugative; **Figure S5B-D**), leading to speculation about their biological role in mediating inter-plasmid conflicts [8,10,12,29]. The targeted plasmids, which are predominantly found in *Klebsiella* and span various Inc groups, are often replicon cointegrates such as IncFII/IncFIB (**Figure S5E-G**). Of particular importance, they commonly harbor multiple antimicrobial resistance genes (57%; **Figure S5H, I**).

We reasoned that plasmid competition mechanisms may act on the horizontal or vertical inheritance of other plasmids, compromising their long-term stability in bacterial populations. To test whether type IV-A3 can mediate inter-plasmid competition, we leveraged three

experimental setups to explore the impact of type IV-A3 targeting on pKJK5, a broad-host-range IncP-1 antibiotic-resistance plasmid (**Figure 3A-E**)[30,31]. We designed crRNAs targeting both DNA strands of pKJK5 in selected regions involved in plasmid replication (replication initiation, *trfA*), inheritance (partitioning, *parA*), conjugation (transfer initiation, relaxase *traI*, and origin of transfer, *oriT*), and expression of a heterologous green fluorescent protein (*gfpmut3*, hereafter *gfp*) (**Figure 3A**, **Figure S6A-C**).

We first asked whether plasmid targeting could limit pKJK5 establishment in a type IV-A3-expressing recipient strain ($R_{IV\text{-}A3}$) upon conjugation from a donor strain (D_0) (**Figure 3B**). When targeting the *trfA* gene, which is essential for plasmid replication, conjugation efficiency was reduced by over four orders of magnitude, while targeting the non-essential sites had no effect on pKJK5 establishment (**Figure 3B, Figure S6D**). Notably, >95 % of transconjugants with targeted *gfp* did not emit green fluorescence, supporting the interference mechanism by transcriptional repression proposed for type IV-A1 (**Figure 3C**)[14] . We then investigated whether targeting pKJK5 in type IV-A3-expressing donors ($D_{IV\text{-}A3}$) could hinder its transfer to a recipient strain (R_0) **(Figure 3D).** Targeting the *oriT* and the *traI* gene, which are required for conjugation, substantially reduced horizontal plasmid transfer (**Figure 3D, Figure S6E**). This is in contrast to the plasmid-incoming experiment, where targeting the same regions did not affect conjugation efficiencies (**Figure 3B, Figure S6D**). Finally, we tested whether type IV-A3 interference could destabilize pKJK5 in a plasmid stability assay (4 days; ~40 generations) in the absence of pKJK5-specific selection. In this assay, pKJK5 was only lost when targeting the *trfA* gene, confirming its essentiality (**Figure 3E, Figure S6F**). We further explored whether type IV-A3 targeting incurred a growth disadvantage on cells with a targeted plasmid, as shown for anti-plasmid systems that function through abortive infection [32,33]. However, there was no qualitative difference in population growth upon targeting (**Figure S6G**). Our experiments demonstrate that type IV-A3 CRISPR-Cas can effectively limit both the transfer and stability of natural conjugative plasmids in bacterial populations, regardless of the targeted strand, and are consistent with a natural CRISPRi mechanism.

IV-A3 interferes with phage propagation

A small fraction of spacers in type IV CRISPR arrays are predicted to match phage sequences (**Figure 1E**, **Figure S2, S5A**) [8,10,11], suggesting a selective advantage for plasmids to retain these spacers. To evaluate this, we challenged *E. coli* with phage λ-vir and designed type IV-A3 crRNAs against both DNA strands of the λ-vir genome at four selected positions, including early and late expressed genes, and an intergenic region (**Figure 3F**). Type IV-A3 interference reduced the ability of λ-vir to propagate in its host for up to five orders of magnitude (**Figure 3G**). Interestingly, interference with phage infection was significant but less pronounced when targeting an intergenic region (**Figure 3G**). These results indicate that type IV-A3 CRISPR-Cas systems can robustly target phages and suggest that type IV-A3-carrying plasmids can enhance their own fitness by protecting their hosts from phage predation.

IV-A3 interference requires the presence of a target interference motif

Mutational evasion of CRISPR-targeting by phage evasion has provided valuable insights into the mechanistic constraints of CRISPR-Cas systems, revealing that the PAM and seed (PAM proximal region, important for initiating target identification) in the protospacer are essential for interference [34–36]. To deepen our mechanistic understanding of type IV-A3 targeting, we isolated and analyzed a set of λ-vir variants capable of escaping interference. We found λ-vir evaded targeting by mutations in the 2nd adenine or the guanine of the 5'-AAG-3' PAM, in the PAM-adjacent region (indicative of a seed region), or by entirely deleting these regions (**Figure S7A-D**), altogether suggesting a reliance on the stringent recognition of a target interference motif (TIM).

To further characterize the TIM requirements of type IV-A3, we used the targeting-deficient type IV-A3 (Δ*dinG*) in an *in vitro* cell-free transcription-translation (TXTL) assay for PAM determination (PAM-DETECT). This restriction enzyme-dependent depletion of protospacer sequences without a recognized TIM [37] revealed a pronounced dependence of the interference complex on the recognition of a 5'-AAG-3' TIM for protospacer binding **(Figure 3H)**. The identified TIM exhibits striking consistency with the 5'-AAG-3' SAM determined in our Cas1/2e-dependent acquisition experiments (**Figure 3H, Figure 2E**), highlighting the compatibility in functional requirements between the type I-E adaptation machinery and type IV-A3 interference complex. Finally, we found that λ-vir also overcame interference through deletion of the region encoding the targeted lysozyme gene *R,* and subsequently acquiring a functional homolog present in other coliphages (**Figure S7E**). Together, these results highlight the strong selective pressure exerted by type IV-A3 interference with λ-vir and the stringent recognition of a TIM for effective targeting.

DinG is essential for blocking expression once transcription has initiated

The above results and a recent study suggest that type IV-A systems elicit target interference through transcriptional repression [14], shedding light on the targeting mechanism. However, the role of the associated DinG helicase remains unclear despite the reported ATP-dependent 5'-3' DNA helicase activity on the target [7,9,13] and its essentiality in this process [11,14]. To shed light on the relevance of DinG during interference, we used three variants of the type IV-A3 CRISPR-Cas system: wildtype, a DinG knockout mutant (Δ*dinG*), and a catalytically inactive helicase mutant (D215A/E216A, *dinGmut;* **Figure 4A**)[11].

We then assessed the ability of the variant systems to target fluorescent reporter genes at various intragenic positions and promoter sites, using an *in vivo* setup (chromosomal *mCherry*; **Figure 4B**) and an *in vitro* TXTL setup (*degfp*; **Figure S8A-B**). Using the wildtype IV-A3 CRISPR-Cas system, targeting within the open reading frame of the reporter genes consistently resulted in a robust decrease of fluorescent signal (**Figure 4C**; **Figure S8C**). In contrast, interference was completely abolished in the absence of DinG (Δ*dinG*)*,* supporting its requirement for gene silencing. With the *dinGmut* variant, we found a reduced mCherry signal when crRNAs hybridized to the template strand but not when crRNAs hybridized to the

coding strand *in vivo*. Targeting in the promoter region, however, always resulted in a strong reduction of reporter signal, independent of the DinG variant (**Figure 4C, Figure S8C**). Indeed, we found that purified type IV-A3 complexes bound strongly (at a low nM apparent dissociation constant K_D) to a cognate double-stranded DNA target in the absence of DinG (**Figure S8D-F**). This shows that initial DNA target binding is independent of DinG and suggests that the reduced reporter signal, observed upon targeting the promoter region of *mCherry* (**Figure 4C**), arises from blocked transcription initiation upon type IV-A3 ribonucleoprotein complex binding. To confirm the transcriptional interference mechanism, we performed RNA sequencing of *E. coli* expressing the WT or Δ*dinG* IV-A3 variants, targeting both strands within *mCherry*. Illumina RNA-seq coverage plots show that mCherry expression is indeed drastically reduced upon targeting by WT but not Δ*dinG* IV-A3 (**Figure S9**). Although the coverage plots show no clear transcriptional effect on neighbouring genes, the upregulation of the distantly encoded pho regulon (**Figure S9**) indicate subtle polar effects over the adjacent *pstS gene*, as mutations in *pstS* have shown to cause upregulation of the pho regulon [38,39]. Together, these results indicate that DinG is crucial to mediate gene repression in transcribed regions and underscore the need for further investigation of IV-A3's polar effects and DinG's processivity in future studies.

IV-A3 mediated re-sensitization of antibiotic-resistant bacteria

Due to the growing spread of antimicrobial resistance in pathogenic strains and its impact on global health [40], there is an urgent need to develop alternative strategies such as restoring antimicrobial susceptibility [41–43]. Our findings highlight that type IV-A3 shows promise as a programmable tool for transcriptional repression, which is particularly noteworthy given the natural propensity of type IV-A3 systems to target conjugative multidrug-resistance plasmids carried by clinical pathogens (**Figure S5F, H-I**).

To investigate the suitability of type IV-A3 for re-sensitizing bacterial strains to antimicrobials, we guided the effector complex towards β-lactam resistance genes (**Figure 4D**). By targeting the ESBL-gene ($bla_{CTX\text{-}M15}$) encoded on the clinical *E. coli* plasmid p1ESBL (**Figure 4E**) [44,45], we restored the strain's susceptibility to the extended-spectrum β-lactam antibiotic ampicillin (Amp). Importantly, the targeted plasmid was maintained in re-sensitized cells, consistent with the transcriptional repression mechanism (**Figure 4E**). With a broth microdilution minimum inhibitory concentration (MIC) assay, we further demonstrated that targeting the chromosomal $bla_{SHV\text{-}187}$ in *K. pneumoniae* 808330 reduced the MIC value below the EUCAST clinical susceptible breakpoint (8 mg/L for Amp, v13.0, 2023-01-01; **Figure 4F**). The resistance reduction was similar to that caused by the SHV-187 null-mutation (Δ*SVH*) (**Figure 4F**) or the addition of the β-lactamase inhibitor clavulanic acid in a disk diffusion assay (**Figure S10A-B**). Together, our results underscore the programmability of type IV-A3 systems for silencing target genes of interest and exemplify their use for combating antimicrobial resistance.

Discussion

CRISPR-Cas systems encoded on MGEs frequently lack adaptation modules [29,46–48] and how they acquire new spacer memory has remained enigmatic. Our experiments support a model in which type IV-A3 CRISPR-Cas systems can overcome this limitation by employing host-derived I-E Cas1/2e proteins). Since the adaptation machinery has a strong preference for sampling MGEs [49], type IV systems may reduce plasmid self-targeting costs while enabling acquisition occasionally, when compatible adaptation modules become available *in trans*. Our findings reveal a striking functional overlap in PAM recognition preferences between the type I-E adaptation and type IV-A3 interference complexes (SAM and TIM, respectively). This highlights the remarkable co-evolution of DNA motif specificity among different but coexisting CRISPR-Cas types, emphasizing their interconnected evolutionary paths. We speculate that other mobile CRISPR-Cas systems, including CRISPR-associated transposons [47,50–52] and certain phage- [48,53,54] and plasmid-encoded loci [29], may similarly co-opt host adaptation machinery to acquire spacer content. Furthermore, a growing body of work is revealing the frequent carriage of diverse anti-phage defense systems by MGEs [55,56], suggesting that functional complementarity with chromosomal loci may be a widespread phenomenon beyond CRISPR-Cas. However, such intricate interactions remain to be investigated in native systems upon MGE entry into the cell.

Despite growing evidence that type IV-A CRISPR-Cas systems are primarily involved in inter-plasmid conflicts [8–10], this hypothesis has remained unexplored. Our findings demonstrate that type IV-A3 can effectively block horizontal transfer and vertical inheritance of conjugative plasmids in bacterial populations by silencing essential plasmid functions. The benefits of licensing interference through non-nucleolytic activities are unclear. However, in contrast to nucleolytic CRISPR-Cas systems, transcriptional repression may be less likely to trigger DNA-damage-induced SOS response that impairs host growth [57–59] and plasmid fitness [60]. This advantage may extend to other MGE-encoded CRISPR-Cas systems lacking nuclease activity, such as types V-M [54] and V-C [61], the helicase-associated type I-C variant [48], as well as other type IV systems [8].

Non-nucleolytic interference may present further advantages, including the capacity to acquire spacers that target chromosomal genes without causing toxic effects. Furthermore, this mechanism could allow plasmids to selectively retain spacers that manipulate the host's or other co-residing MGE's transcriptional profiles to their advantage. In support of this, Guo et al. 2022 reported the repression of the chromosomal pilus biogenesis gene *pilN* by a plasmid-encoded type IV-A1 system. Interestingly, a significant proportion of type IV CRISPR spacers match plasmid conjugation genes [8], which are also involved in pilus formation. For example, phages using pili as receptors are widespread [62], and it is possible that type IV-driven pili repression enhances plasmid fitness by preventing phage entry into host cells.

Albeit dependent on the presence and catalytic integrity of DinG, we demonstrate that type IV-A3 can robustly interfere with transcription initiation and elongation when targeting both the coding and template strands. Notably, strand-independence greatly increases the number of available PAMs and highlights the potential of type IV-A3 as a CRISPRi tool that contrasts the conventional nuclease-deficient Cas9 (dCas9) [63,64], dCas12 [65,66] and Cascade [67], which are mostly restricted to the coding strand. As a proof-of-concept demonstration, we show that type IV-A3 gene silencing can be repurposed to re-sensitize bacteria to antibiotics, including high-risk clinical *K. pneumoniae* strains resistant to last resort β-lactams [68]. We further showcase that the targeting of plasmid-encoded accessory genes does not cause plasmid loss, highlighting the distinctive potential of type IV-A3 to lower the risk for emergence of CRISPR-Cas inactivating mutations [69,70]. Indeed, such unwanted mutations are particularly favored when targeting natural plasmids for removal, as they frequently encode addiction systems that select for their maintenance in the population [71,72]. We anticipate that further investigations of the molecular mechanisms underlying type IV CRISPR-Cas systems will present further opportunities for harnessing their unique crRNA-guided properties in biotechnological applications.

Acknowledgment

We thank the Synthetic Biology and Microbial Evolutionary Genomics groups at Institut Pasteur, the Section of Microbiology at the University of Copenhagen, the Phi Lab (Peter Fineran's group) at Otago University, and the Pathogen Ecology group at ETH Zürich for helpful discussions and mimosas. We thank David Mayo-Muñoz for valuable feedback on the manuscript and Ekaterina Semenova for help with the design of acquisition experiments. We thank Sylvain Brisse (Institut Pasteur) for providing *K. pneumoniae* strain SB and his group, especially Carla Rodrigues and Chiara Crestani, for help with Oxford Nanopore sequencing. We thank Azimdine Habib, Laure Lemée and Thomas Cokelaer from the Biomics Platform (C2RT, supported by France Génomique ANR-10-INBS-09 and IBISA) at Institut Pasteur for help with RNA sequencing and corresponding analysis in transcriptional repression assays. Plasmids encoding P70A-deGFP and P70A-T7RNAP were kindly provided by Prof. Vincent Noireaux. We thank the Šikšnys laboratory (Vilnius University) for providing access to the Octet K2.

F.B. was supported by the SNSF [grants P1EZP3_195539 and P500PB_210944]. S.C.-W. was supported by the Lundbeck Foundation grant [J.S.M., R250-2017-1392]. M.A.-A was supported by HORIZON-MSCA-2021-PF-01–01 and EvoPlas-101062386. L.R. was supported by DFG-SPP2141 and the LOEWE Research Cluster Diffusible Signals. J.S.M was supported by the Independent Research Fund Denmark [0217-00445B]. R.P.-R. was supported by a Lundbeck Foundation grant [R347-2020-2346]. P.P. receives funding from the European Regional Development Fund under grant agreement number 01.2.2-CPVA-V-716-01-0001 with the Central Project Management Agency (CPVA), Lithuania, and from the Research Council of

Lithuania (LMTLT) under grant agreement number S-MIP-22-10. A.C. was supported by the two Cantons of Basel [grant PMB-03-17] and by the SNSF [grant P500PB_214356]. S.J.S. was funded by the Novo Nordisk Foundation PEACE project 0064822. L. M. was supported by the European Union's Horizon 2020 research and innovation programme under Grant No. 874735 (VEO). K.W., F.E. and C.B. were supported by the Deutsche Forschungsgemeinschaft (BE 6703/1-2 to C.L.B.).

Author contributions

R.P.-R., F.B, and S.C.-W. conceived the project.
J.V.G.F. performed RNA-seq for validation of CRISPR-Cas processing activity, F.B. and M.R.M. performed RNA-seq for IV-A3 mediated transcriptional repression, K.W. and F.E. performed TXTL and TIM assays, A. C. identified *K. pneumoniae* 808330. R. Č. expressed and purified ribonucleoprotein complexes and performed BLI. The other experiments were performed by F.B., S.C.-W, J.K., and S. G..
F.B., S.C.-W., K.W., F.E., J.V.G.F., J.K., S. G., and L.M. verified the overall reproducibility of results and other research outputs.
M. A. -A., M.R.M., and J.R. implemented bioinformatic analyses.
M. A. -A., J.R., M.R.M., F.B., M.A.S, R.P.-R., and S.C.-W. performed computational analyses.
J.R., M. A. -A., M.R.M., F.B., and S.C.-W. analyzed and synthesized study data by applying statistical, mathematical, and computational techniques.
R.P.-R, F.B., and S.C.-W. curated data.
R.P.-R., F.B., and S.C.-W. wrote the initial draft of the manuscript and designed figures.
All authors revised and crucially contributed to the current draft of the manuscript.
R.P.-R. managed and coordinated research activity planning and execution.
R.P.-R., P.P., C.B., D.B., A.H., S.J.S., J.S.M., L.R., and E.R. provided mentorship and oversight of the research activities.
Funding acquisition by R.P.-R, F.B., A.H., J.S.M., D.B., C.B., S.J.S, P.P., and L.R.

Declaration of interests

The authors declare no competing interests.

Main Figures Titles and Legends

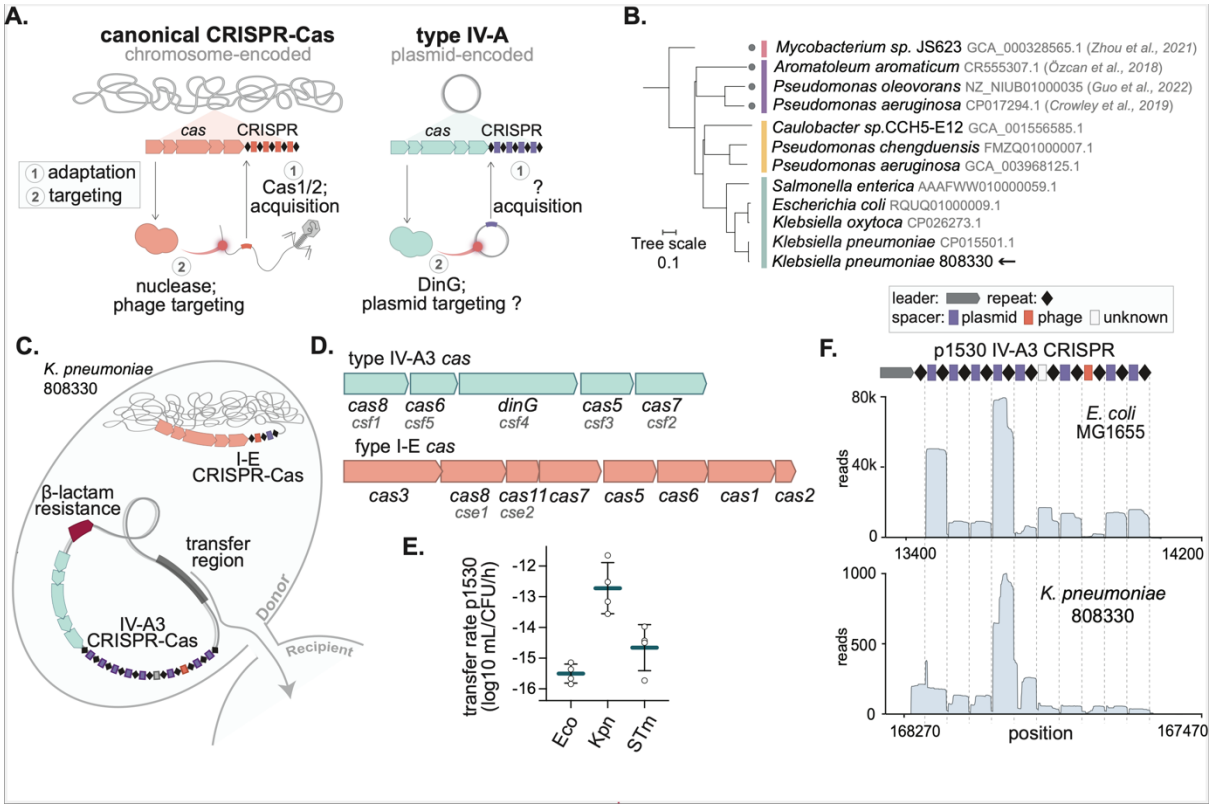

Figure 1: The *K. pneumoniae* type IV-A3 CRISPR-Cas system encoded on a conjugative ESBL-plasmid is functionally active. A) Comparison of canonical CRISPR-Cas systems (left) and type IV-A CRISPR-Cas (right). Most CRISPR-Cas systems are chromosomally encoded, contain Cas1/2 to acquire new spacers, and primarily target phages using associated nucleases. Type IV-A CRISPR-Cas are encoded on conjugative elements such as plasmids, lack Cas1/2 modules and carry a DinG helicase instead of a nuclease component. **B)** Phylogenetic tree showing the selected type IV-A3 from *K. pneumoniae* 808330 (arrow) among other type IV system representatives. Previously studied orthologs and taxonomic assignments of their hosts are indicated (gray dot). The phylogenetic tree was built using Csf2 (Cas7) protein alignments. **C)** Schematic of *K. pneumoniae* 808330 with the plasmid encoded type IV-A3 and chromosomal type I-E systems. **D)** Schematics of the *K. pneumoniae* 808330 IV-A3 and I-E *cas* operons. **E**) Mean rates of p1530 conjugation (blue lines) from its native host *K. pneumoniae* 808330 to different *Enterobacteriaceae* species: *E. coli* (Eco), *K. pneumoniae* (Kpn), and *Salmonella enterica* Typhimurium (STm). The error bars indicate the SD (n=4). **F)** Schematic of the type IV-A3 CRISPR array carrying ten spacers (top), with their predicted origins indicated in purple (plasmid), orange (phage), or white (unknown). Small RNA-sequencing of the type IV-A3 CRISPR-Cas locus expressed in *E. coli* MG1655 (middle) and *K. pneumoniae* 808330 (bottom) mapped back to the p1530 CRISPR array (x-axis).

See also Figure S1-S3.

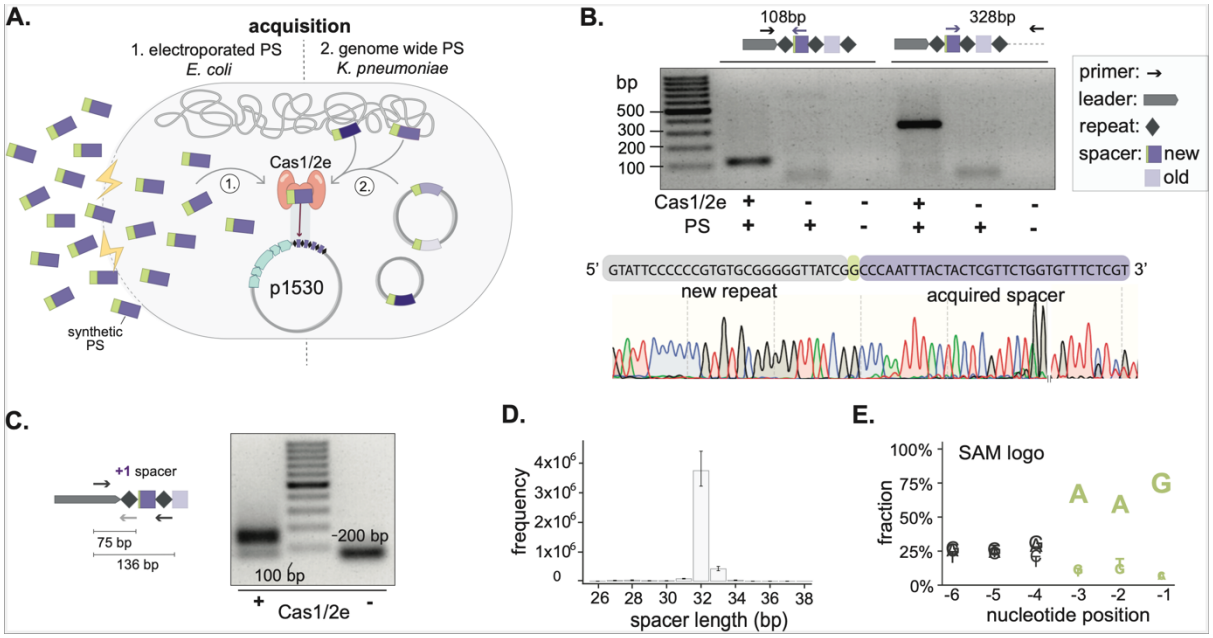

Figure 2: Type I-E adaptation machinery facilitates spacer acquisition in type IV-A3 CRISPR loci. A) Schematic of the two acquisition experiment setups. Experiment 1: *E. coli* harboring the p1530-encoded type IV-A3 CRISPR-Cas system and electroporated with double-stranded DNA protospacers (PS, purple) with a 5'-AAG-3' SAM (green). Experiment 2: *K. pneumoniae* with a targeting-deficient p1530-encoded type IV-A3 system. In both experiments, the Cas1/2e adaptation module was expressed from a plasmid. **B)** Experiment 1: The PCR schematics and gelshow the amplification of the CRISPR array downstream (left) and upstream (right) of the newly acquired spacer. Below the corresponding Sanger result where the trace indicates the assembly of sequences from opposing directions. **C)** Experiment 2: Detection of Cas1/2e-dependent genome-wide spacer acquisition in *K. pneumoniae* by PCR and amplicon deep-sequencing. The PCR schematic and gel show the amplification during the second step of CAPTURE PCR of the leader-proximal end, 136 bp for elongated arrays (left) and 75 bp for the leader amplification (right). Black arrows indicate primer annealing sites and the gray arrow indicates a secondary binding site. **D)** Mean number of integrated spacers by length (x-axis) as bars with error bars indicating the 95 % confidence interval (n=3). **E)** Sequence logo of the SAM as determined by the genome-wide spacer acquisition assay. Nucleotide abundance is shown as the mean fraction (n=3) at positions -6 to -1 of the acquired 32 bp-spacers.

See also Figure S4.

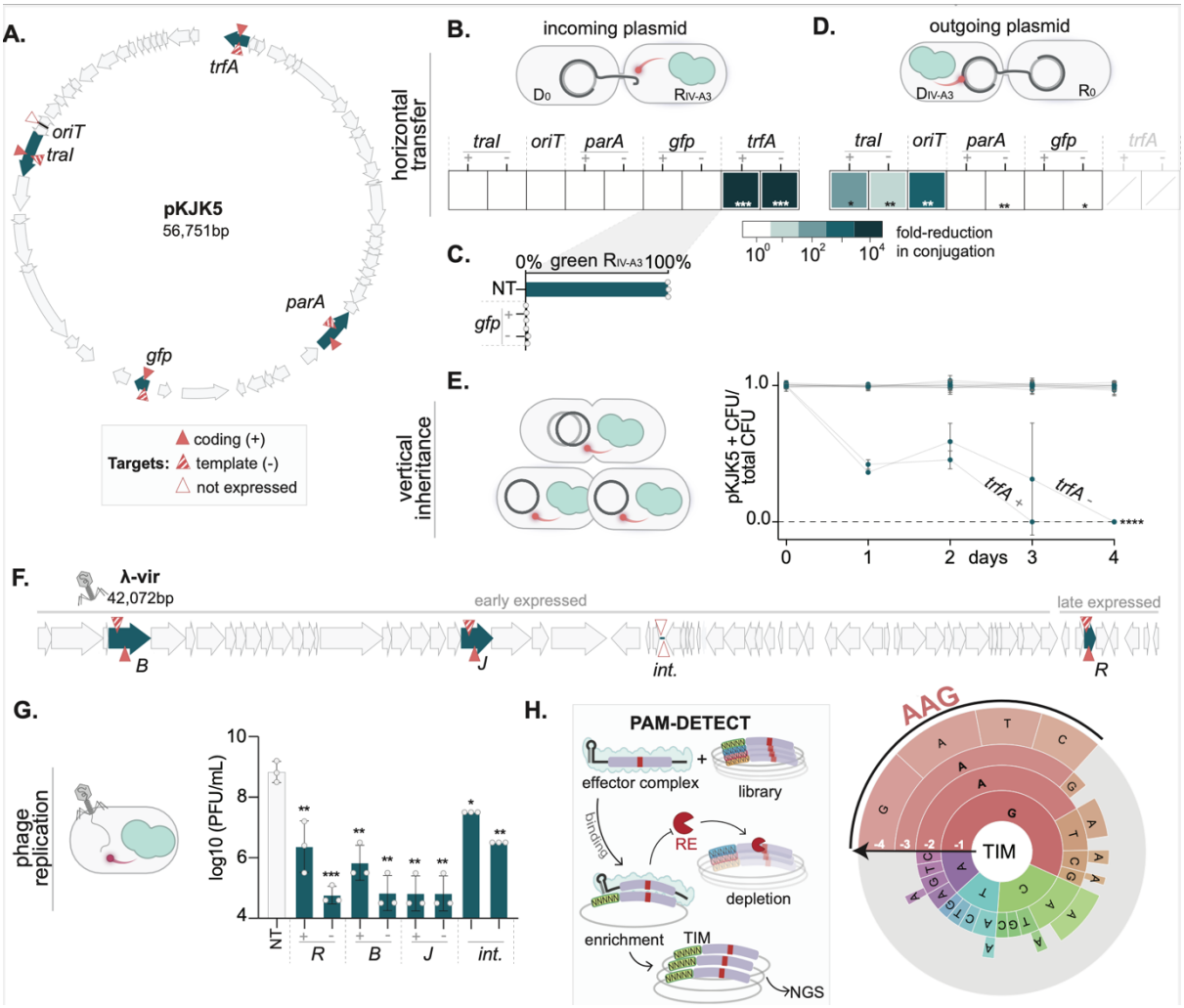

Figure 3: Type IV-A3 mediates crRNA-directed interference with conjugative plasmids and phages. **A)** Gene map of pKJK5 indicating the regions targeted by type IV-A3 in blue. Red triangles represent the approximate location of protospacers. **B)** Type IV-A3 interference in *E. coli* recipients R_{IV-A3}. **C)** Evaluation of GFP fluorescence under type IV-A3 targeting in R_{IV-A3}. Bars represent the mean of transconjugants emitting green signals, comparing a non-targeting (NT) crRNA control to crRNAs targeting *gfp.* **D)** Type IV-A3 interference in *E. coli* donors D_{IV-A3}. Evaluation of *trfA* targeting was not feasible due to the instability of pKJK5 while expressing type IV-A3 CRISPR-Cas (crossed, gray-shaded squares). The conjugation efficiency of pKJK5 in **B** and **D** is shown as the conjugation reduction compared to the NT control. **E)** Plasmid maintenance assay showing pKJK5 stability under type IV-A3 targeting in the absence of pKJK5-selection over ~40 generations. The dotted line indicates the detection limit of the assay. Blue dots show the mean of four biological replicates with error bars as SD (n=4). **F)** Genome map of λ-vir indicating the regions targeted by type IV-A3 in blue. Target sites are shown as in **A**. Early and late expressed regions are indicated. **G)** Type IV-A3 interference of λ-vir infection in *E. coli* determined as plaque forming units (PFU)/ mL. Bars show the mean values and error bars indicate the SD. **H**) Schematic of PAM-DETECT method on the left. TIM wheel on the right shows the mean sequence motif recognized by type IV-A3 interference complex in 5' > 3' from outer to inner position (n=2). In the TIM wheel, sequences radiate from the inner to the outer circle, matching the direction of the TIM read from the protospacer. Colors represent the relative frequency of the nucleotide in the inner circle. The size of the arc for each nucleotide position corresponds to its relative enrichment within the TIM library. Individual sequences comprising at least 2 % of the PAM wheel are

shown. P values in panels **B** and **D-F** represent two-sample Student's t-Tests of log10 transformed T/(R+T) for panels **B** and **D**, pKJK5^{+} fraction for **E** and PFU/mL for **G**, comparing each targeting treatment to the NT control (n=3 if not stated otherwise). **** P ≤ 0.0001; *** P ≤ 0.001; ** P ≤ 0.01; *P ≤ 0.05.

See also Figure S5-S7.

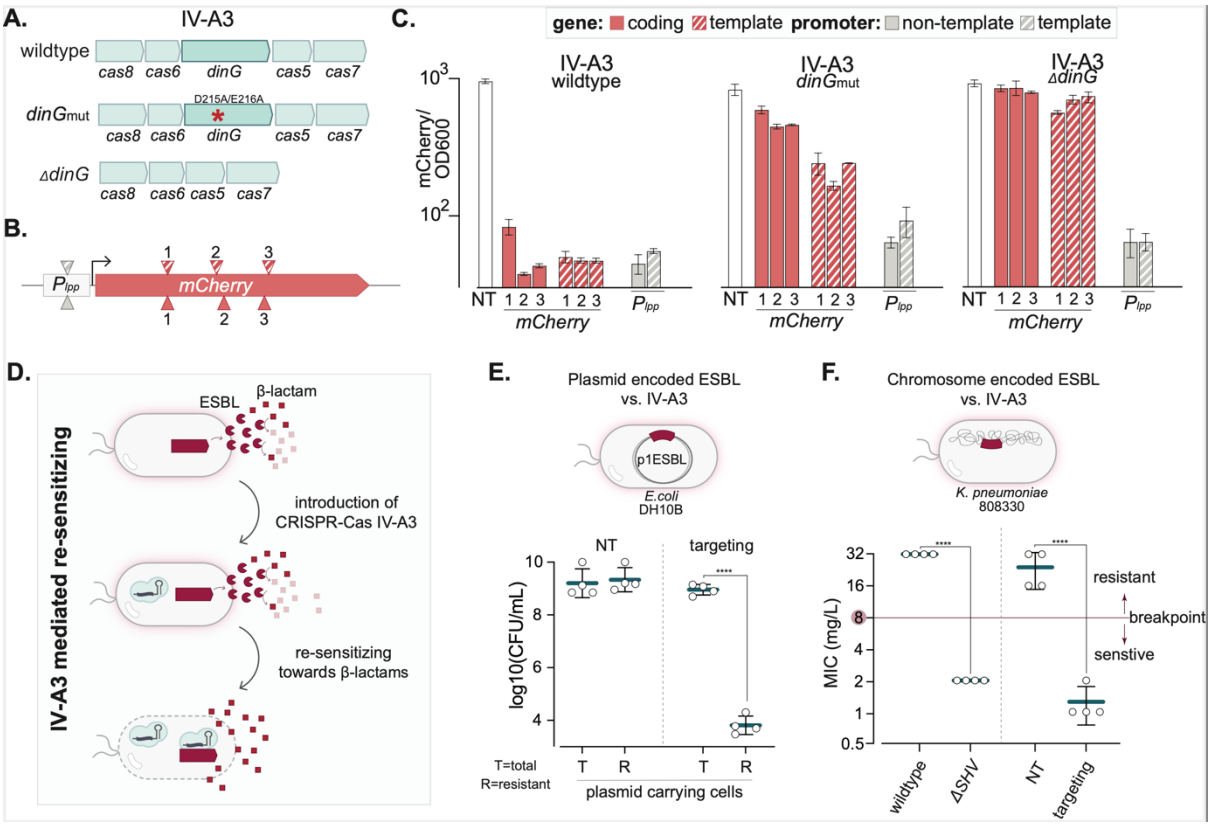

Figure 4: Type IV-A3 interference functions through transcriptional repression and can re-sensitize antibiotic-resistant bacteria. A) Schematic of the three type IV-A3 CRISPR-Cas variants used in the *mCherry* reporter targeting assay; wildtype, *dinGmut* with a catalytically inactive DinG, and the Δ*dinG* knockout mutant. **B)** Illustration of the mCherry reporter construct. Triangles represent the approximate location of protospacers within *mCherry* (red) and the P_{lpp} promoter (gray), where the crRNA hybridizes to the coding (full) and template (crosshatched) strands **C)** *In vivo* transcriptional repression assay. The mean mCherry fluorescence signal is normalized to bacterial OD_{600} (y-axis) and the targeted positions are shown on the x-axis. Error bars indicate SD. A linear model indicated that IV-A3 variant, target position (promoter vs. gene), and strand significantly contribute to relative mCherry levels (R^2 = 0.98, P < 0.0001 for all factors) and a bidirectional stepwise linear regression that target position is the most important predictor, followed by IV-A3 variant, and then strand (n = 3) . **D)** Diagram illustrating the process of restoring β-lactam sensitivity in ESBL-producing strains through crRNA-guided type IV-A3 CRISPR-Cas gene silencing. **E)** Reversal of ESBL-mediated antibiotic resistance encoded on p1ESBL carried by *E. coli* DH10B shown as the $\log_{10}$ of colony forming units (CFU)/ mL under type IV-A3 interference (targeting) and the NT control. Lines represent the mean of the plasmid-carrying cells: total population of plasmid-carrying cells (T) and the β-lactam resistant subpopulation thereof (R) (n= 4). Error bars indicate the SD. **F)** MIC of Amp for *K. pneumoniae* 808330 under type IV-A3 mediated transcriptional repression of $bla_{SHV\text{-}187}$ (right) and for a Δ*SVH* mutant (left). The EUCAST

susceptibility breakpoint (8 mg/L) is indicated in red. Datapoints shown at 32 mg/L are ≥ 32 mg/L and error bars indicate SD. The p-value in panels **E** and **F** represents a two-sample Student's t-Tests, of the $\log_{10}$ transformed CFU/mL for E and MIC values for F (n = 4 for both). **** P ≤ 0.0001.

See also Figure S8-S10.

STAR METHODS

1. RESOURCE AVAILABILITY

Lead contact

Further information and requests for resources and reagents should be directed to and will be fulfilled by the lead contact, Rafael Pinilla-Redondo (rafael.pinilla@bio.ku.dk).

Materials availability

All materials generated in this study are available upon request from the lead contact, Rafael Pinilla-Redondo.

Data and code availability

All data generated in this study are publicly available as of the date of publication, DOIs and accession numbers are listed in the key resource table. Standardized data types (sequencing datasets) are available from Genebank (BioProject PRJNA1066244), all other data types (raw data) are deposited on Dryad under https://doi.org/10.5061/dryad.8pk0p2nvp. Analysed plasmid sequences are freely available at RefSeq (state March 2021).

This paper does not contain original code. All softwares and algorithms used in this study were previously described and are listed in the key resource table.

Any additional information required to reanalyze the data reported in this paper is available from the lead contact upon request.

2. EXPERIMENTAL MODEL AND STUDY PARTICIPANT DETAILS

Bacteria

Bacterial strains are listed in the key resource table. Unless stated otherwise, bacterial cultures grew at 37 °C and under agitation (180 rpm) in lysogenic broth (LB) medium, supplemented with appropriate amounts of antibiotics: none, 100 μg/mL carbenicillin to maintain plasmid pMMB67he, pYTK095, p1530 and derivatives thereof; 25 μg/mL chloramphenicol (CM) to maintain plasmid pMMB_IVA3_Cas_Cm or select for CM resistant MG1655; 20 μg/mL gentamicin to maintain plasmid pHERD30T and derivatives; 20ug/mL kanamycin or 15 μg/mL tetracycline to maintain pKJK5 and 50 μg/mL to select for pRSF-derivates. When appropriate, the following inducer concentrations were used: 0.2–0.3 % w/v L-arabinose and 0.1 mM isopropyl β-D-1- thiogalactopyranoside (IPTG). We stored isolates in 25% glycerol at −80 °C.

Phage

To propagate the virulent *E. coli* phage λ-vir, we incubated a single plaque with *E.coli* GeneHogs in 3 mL of LB containing 10 mM MgSO4 at 37 °C for 3 h. Then we added the 3 mL phage-bacteria mix to a 20 mL culture of *E.coli* GeneHogs of an optical density (OD at 600 nm,

hereafter OD600) of ~0.8, which we incubated at 37 °C for 6 h or until clear. We collected phages by sterile filtering the lysate and storing it at 4 °C over chloroform.

3. METHOD DETAILS

Analysis and whole genome sequencing of *K. pneumoniae* 808330 genome

We screened the *Klebsiella spp.* collection from the University Hospital Basel, Switzerland to identify *K. pneumoniae* 808330, which was isolated in 2017 from a rectal swab taken during a hospital hygiene screening. We performed library preparation for *K. pneumoniae* 808330 with a Nextera XT Kit to sequence on an Illumina NextSeq500 (paired end, 2 × 250 bp) and a rapid barcoding sequencing kit (SQK-RBK004). We then proceeded to sequence with an Oxford Nanopore MinION system (FLO-MIN-106 flow cell). To generate a hybrid assembly, we used Unicycler v0.4.8 [73] and annotated CRISPR-Cas systems using CRISPRCasTyper (v1.8.0) [74], plasmids with Plasmidfinder and MOB-suite [75,76], and resistance genes by blasting against the CARD database [77].

p1530 transfer rate estimation

To estimate p1530 transfer rates [mL (CFU h)$^{-1}$], we used the Approximate Extended Simonsen Model, which accounts for varying growth rates of donor, recipient, and transconjugants and estimates a time window for reliable transfer rate estimations [78]. The p1530 plasmid transferred from its native host *K. pneumoniae* 808330 to the clinical *E. coli* Z1269 and *K. pneumoniae* SB5442, both carrying the Cm resistance-plasmid pACYC184, and to STm 14028 with the chromosomal Cm marker *marT::cat.* In brief, we grew four independent overnight cultures of donor and recipient strains supplemented with appropriate antibiotics, washed them by pelleting and resuspending, and mixed 1µL of 6.5-fold diluted donor and recipient cultures each to 150µL LB in a 96-well plate (final 1000-fold dilution). We enumerated donors, recipients, and transconjugants in mating populations after 6 h of growth without agitation, and estimated their growth rates (h^{-1}) based on hourly OD600 measurements (Tecan NanoQuant Infinite M200 Pro) using the R package Growthcurver. Finally, we estimated transfer rates with the R package conjugator [78].

Cas7 phylogenetic tree

We selected a representative set of type IV-A CRISPR-Cas systems and used CRISPRCasTyper (v1.8.0) [74] to extract the Cas7 (Csf2) protein sequences. The chosen type IV-A loci covered the diversity observed across the type IV-A variants (A1-A3) [8] and included the reference type IV-A1 systems studied in previous works [5,11,14]. To root the subsequent tree, we used the Cas7 from a previously studied type IV-B system [6]. We then used the online MPI Bioinformatics Toolkit [79] (v.10.10.2023) to perform a multiple sequence alignment, using MAFFT (v.7.0) (Gap open penalty: 1.53; Gap extension penalty: 0.123) [80]. We then created a maximum-likelihood phylogenetic tree and calculated the bootstrap values with PhyML (v3.0) [81], using 200 iterations. The resulting tree was visualized with ITOL (v5.0) [82].

Identification of type IV-A3 carrying and targeted plasmids -

Type IV-A3 CRISPR-Cas systems were retrieved by running CRISPRCasTyper (v1.8.0) [74] on the ENA bacterial genome database (April 2023) [83]. To identify IV-A3-encoding plasmids we run CRISPRCasTyper (v1.8.0) [74] on the PLSDB plasmid database [84] (April 2023; **Table S3**). To identify plasmids (and phages) targeted by type IV-A3 systems (i.e, carrying matching protospacers; **Table S4** for plasmids), we first extracted spacers from the identified type IV-A3 CRISPR arrays and dereplicated them using cd-hit-est *(v.4.8.1)* [85] (90% identity and 90% coverage), yielding a dataset of 450 non-redundant spacers. (**Table S5**). We used the BLAST suite of programs, v.2.6.0+ [86] to screen the spacer queries in >55,000 plasmid and bacteriophage sequences. As a plasmid database, we employed the 21,520 plasmids retrieved from the complete genomes available in the NCBI non-redundant RefSeq database (state March 2021). As a bacteriophage database, we used the 34,718 bacteriophage sequences available in the NCBI Virus Collection (state June 2023). We indexed both databases with makeblastdb (default parameters) and used blastn (v.2.6.0+) to screen for matching protospacers, with the option -task blastn-short and an E-value threshold of 0.05 given the short length of the queries. Hits against type IV-A3-encoding plasmids were discarded to avoid potential matches against type IV-A3 CRISPR arrays. Moreover, we only retrieved hits showing >95 % identity and >95 % coverage for further analysis. This resulted in a total number of 3,046 hits, 3,035 against the plasmid database, and 11 against the phage database. The total number of unique spacers with hits in the databases was 71. 58% showed 0 mismatches in the alignment, and 42% showed one mismatch. No alignment with >1 mismatch was retrieved.

Characterization of type IV-A3 carrying and targeted plasmids

As a plasmid database, we used 21,520 plasmids retrieved from the complete genomes available in the NCBI non-redundant RefSeq database (March 2021) and as a bacteriophage database, the 34,718 sequences available in the NCBI Virus Collection (June 2023). For both, type IV-A3 carrying and targeted plasmids, we identified plasmid incompatibility groups with PlasmidFinder, v.2.0.1 [75], using the database of *Enterobacterales* (v.2023-01-18), and antimicrobial resistance genes with the software AMRFinderPlus, v.3.11.4 [87]. Additionally, some of these plasmids have previously been characterized as phage-plasmids [88]. Finally, to characterize the mobility of plasmids we identified Mating Pair Formation (MPF) system and relaxase (MOB) with CONJScan, v.2.0.1 [89], and oriT with an in-house protocol previously described [90]. The MPF, MOB, and oriT allowed us to classify plasmids as conjugative (putatively complete MPF system with a relaxase), decay conjugative (incomplete MPF system with a relaxase), MOB-mobilizable (relaxase in the absence of an MPF system), and oriT-mobilizable (presence of an *oriT* and absence of both MPF and MOB). The remaining replicons were considered as non-transmissible. To visualize this data we used the R package ggplot2, v.3.3.5 [91], with the addition of the R packages UpSetR, v.1.4.0 [92] and ggridges, v.0.5.3 [93] where required.

Design and cloning of expression vectors

For the construction of expression vectors we performed USER cloning (NEB) or Gibson Assembly (NEB) following the manufacturer's instructions. For exchanging the spacer sequences in pHerd_IV-A3_mini-array_NT we used Golden Gate DNA Assembly or restriction cloning, digesting 500 ng of the backbone with *Bsa*I-HF (NEB) and ligating 5 µL of 5 µM spacers (annealed oligos) with 80ng of *Bsa*I-digested backbone using the T4 ligase (NEB). We chose spacer sequences based on protospacer position and their association with a 5'-AAG-3' motif and annealed them from two oligonucleotides with the according restriction site overhangs (95 °C for 5 min, 23 °C for 15 min). All constructs were then transformed into *E.coli* and constructs were confirmed by Sanger and/ or Oxford Nanopore sequencing. All oligonucleotides used in this study are listed in **Table 57**.

CRISPR-Cas activity: RNA Sequencing and data analysis

To test type IV-A3 activity, we analyzed crRNA processing in both, *K. pneumoniae* 808330 under natural expression from p1530 and in *E. coli* MG1655 from pMMB_IVA3_Cas_CRISPR. For both we extracted small RNAs with the mirVana isolation kit (Ambion), treated with DNase I (New England Biolabs, NEB), end-repaired with T4 Polynucleotide Kinase (NEB), and submitted final products to library preparation (NEBNext Ultra RNA Library Prep Kit for Illumina), following the manufacturer's instructions. For the transcriptomic analysis of *K. pneumoniae* 808330, we extracted total RNA with the mirVana isolation kit (Ambion), treated with DNase I (NEB), rRNA depleted with a NEBNext rRNA Depletion Kit (Bacteria), and submitted final products to library preparation using a NEBNext Ultra II Directional RNA Library Prep Kit for Illumina following the manufacturer's instructions. We sequenced with an Illumina MiniSeq System in single-end mode, generating 150 nucleotide reads and quality control using FastQC (v.0.11.9) [94]. We trimmed reads with Cutadapt (v1.18) and aligned them to the genome of 808330 and *E. coli* MG1655 using Hisat2 [95–97]. To calculate the abundance of transcripts we used the RPKM method [98]. For data analysis, coverage plots, and scatter plots we used the R package ggplot2 [99].

Expression and purification of the type IV-A3 ribonucleoprotein complex

To express the type IV-A3 ribonucleoprotein complex and the crRNA, we grew overnight cultures of single colonies of *E. coli* BL21 Star containing the plasmid-encoded type IV-A3 complex with a C-terminal Gly-His6-tag at Cas7 (Csf2), each in 15 mL terrific broth (TB, Thermo) at 37 °C with required antibiotics and at 200 rpm (here and the following steps). These starter cultures we subcultured in 1 L TB with required antibiotics to an OD600 of 0.6 – 0.8, before induction of expression by adding IPTG and further growth for 3 h. We pelleted cells by centrifugation (3,600 x g, 30 min, 4 °C) and resuspended them in 20 mL lysis buffer (10 mM HEPES-Na, pH 8.0, 150 mM NaCl, 40 mM imidazole) before cell lysis by sonication using a Vibra-Cell ultrasonic processor at 40 % amplitude for 5 min with pulses of 3 s at 3 s intervals. We cleared lysates by centrifugation (47,384 x g for 20 min at 4 °C) and applied supernatants onto 1 mL HisTrap FF columns (Cytiva, pre-equilibrated in lysis buffer, for Ni-NTA affinity chromatography at 4 °C). After a wash step with 15 column volumes of lysis

buffer, we eluted proteins with three column volumes of elution buffer (10 mM HEPES-Na, pH 8.0, 150 mM NaCl, 500 mM imidazole). We concentrated proteins to 0.5 mL at 4 °C and further purified by size-exclusion chromatography using a Superose 6 Increase 10/300 GL column (Cytiva, equilibrated in size exclusion buffer: 10 mM HEPES-Na, pH 7.5, 150 mM NaCl) at 4 °C. We then concentrated main peak fractions to 0.5 mL at 4 °C and estimated concentrations based on the absorbance at 280 nm using a NanoDrop Eight spectrophotometer (Thermo) and extinction coefficients based on an assumed Cas protein complex stoichiometry of 1:1:6:1 (Cas5:Cas8:Cas7:Cas6).

Verification of *in trans* spacer acquisition

A similar approach to detect the acquisition of synthetic protospacers has been used by Shipman et al., 2016 [23]. In brief, we grew *E. coli* MG1655 carrying p1530 in combination with either pHerd_Cas1/2e or pHerd30T_ev (negative control) overnight, each in triplicates, and subcultured cells in LB containing 0.2 % w/v L-arabinose until they reached an OD600 of ~0.4. We made each replicate electrocompetent according to standard laboratory procedures and electroporated 100 ng of the double-stranded protospacer PS (PSA33 [23]) as annealed oligonucleotides. As a negative control, we electroporated cells without any PS DNA. Cells were recovered for 1.5 h in LB supplemented with 0.2 % w/v L-arabinose, spun down and resuspended in 50 µL water, and stored at 4 °C until further processing. To confirm the acquisition of the new PS in the type IV-A3 array, we performed two PCRs on each of these templates: one PCR to amplify the leader-proximal end (pFB29, annealing to PS/pFB39) and one to amplify the leader distal end (pFB28, annealing to PS/pFB74). We verified spacer integration in the leader-repeat junction by agarose gel electrophoresis and PCRs yielded amplicons of 108 bp and 328 bp, respectively. We subjected PCR products from each replicate to Sanger-sequencing twice, once with pFB29 (leader-proximal end) and once with pFB28 (leader-distal end). We performed PCRs with the Phusion DNA Polymerase (Thermo) following the manufacturer's protocol and with an annealing temperature of 60.1°C for 35 cycles.

Detection of spacer acquisition in native CRISPR arrays

To facilitate genome-wide spacer acquisition we used a p1530Δ*dinG* (NT) containing *K. pneumoniae* 808330. We generated this mutant in *E. coli* GeneHogs using the lambda red recombinase system [100]. For the assay, we conjugated p1530Δ*dinG* back into *K. pneumoniae* 808330, from which we previously cured p1530. To test acquisition in the I-E array, we used both the p1530Δ*dinG*-carrying and the p1530-cured versions. We grew *K. pneumoniae* strains from single colonies with pHerd_Cas1/2e or pHerd30T_ev (negative control) in triplicates or quadruplicates in LB supplemented with L-arabinose (0.2 % w/v) overnight. For each sample, we extracted total DNA with the DNeasy Blood &Tissue Kit (QIAGEN) from 1.5 mL cultures, which we used as templates for subsequent PCR reactions (100 ng). To monitor adaptation, we amplified the leader-proximal end of the CRISPR array by CAPTURE PCR [27]: a first PCR with primers targeting the leader (pFB88 for IV-A3/ pFB97 for I-E) and the first spacer (pFB89/ pFB96, spacer1) isolated the leader-proximal end (leader-repeat1-spacer1 for unextended

and leader-new repeat-acquired spacer-repeat1-spacer1 for extended arrays). We separated extended amplicons from unexpanded products by agarose gel electrophoresis (2.5 % w/v), cut invisible bands of elongated arrays (174 bp), and isolated DNAs with the GeneJET Gel Extraction Kit (Thermo). These served as templates for a second PCR: we amplified extended arrays with pFB88/pFB97 and degenerate primers targeting repeat1, whose 5' ends are not complementary to the 3' end of the leader (adenine, pFB90, pFB91, pFB92 for IV-A3 and pFB98, pFB99, pFB100 for I-E). Importantly, this method introduces a bias because spacers that carry the base adenine at their 3' end are likely not amplified. After this selective PCR, we separated expanded/unexpanded amplicons by agarose gel electrophoresis (1.5 % w/v). None of the I-E and one IV-A3 replicates showed a band the size of expanded arrays and thus were excluded from further analysis. We performed PCRs with the Phusion DNA Polymerase (Thermo) following the manufacturer's protocol and with an annealing temperature of 67.2 °C for 35 cycles. To reach a high enough DNA concentration for high-throughput sequencing, we performed each PCR with multiple reactions for each sample. Array-amplicons were sequenced at Novogen (Illumina NovaSeq, 150 nucleotides paired-end reads, UK) after adaptor ligation (NEBNext Ultra II DNA Library Prep Kit for Illumina). After sequencing, we de-multiplexed samples by index and had an average of 4,616,517 read pairs. First, we filtered and trimmed reads according to base qualities with Trimmomatic (v0.39) [101] with the following parameters: PE LEADING:5 TRAILING:5 MINLEN:80 AVGQUAL:20. Filtering removed on average 0.11% of the read pairs. Second, we merged forward and reverse reads with PEAR (v0.9.6) [102] with default parameters. On average 98.35 % of filtered read pairs were merged. To extract spacers we used cutadapt (v1.18) [95] with the pattern (partial leader + *repeat* + spacer(...) + *partial repeat*, or the reverse complement) with the -g option: "GCTGGTGGATTTTAGTGGCGCTATTTAATATTTTATAATCA-ACCGGTTATTTTTAGA*GTATTCCCCCCGTGTGCGGGGGTTATCG*...*GTATTCCCCCCGTGTGCG*".
From on average 93.4 % of merged read pairs a spacer of any length could be extracted, of which 97 % were between 31 and 35 bp. We reverse-complemented spacers extracted with the reverse complement pattern to match the transcribed strand. To align spacers we searched for perfect matches on either strand of present genomes and excluded matches to the array on p1530 and spacers aligning multiple locations; this resulted in matches for 78.5 % of the 32 bp spacers, which we used for the SAM analysis.

pKJK5 targeting assays

To test the type IV-A3's capacity to target the environmental and tetracycline-resistant IncP-1 plasmid pKJK5 tagged with *gfp* [31] in *E. coli*, we overexpressed the IV-A3 Cas operon from the P_{TAC} promoter and complemented it with a crRNA (mini array; repeat-spacer-repeat sequence) expressed from the P_{Bad} promoter crRNAs contained spacers targeting *trfA*, *parA*, *traI*, and *gfp* in the coding (+) and template strand (-), and the *oriT*, and we used the non-targeting pHerd_IV-A3_mini-array_NT as a negative control. Plasmids are given in **Table S6**,

oligonucleotides in **Table S7**, and explanations for a spacer design are provided in **Figure S6A-C**.

With this, we set up three independent targeting assays, two to test type IV-A3 interference with pKJK5 transfer and one to test IV-A3 interference with pKJK5 stability within a bacterial population. In the pKJK5 incoming (from D_0 to $R_{IV\text{-}A3}$) (**Figure 3B**) and the pKJK5 outgoing (from $D_{IV\text{-}A3}$ to R_0) (**Figure 3D**) assays, we estimated IV-A3 interference in the *E. coli* MG1655 recipient $R_{IV\text{-}A3}$ and donor $D_{IV\text{-}A3}$, respectively, as the pKJK5 transfer efficiency ($CFU_{transconjugants}$/ ($CFU_{recipients}$+$CFU_{transconjugants}$), (T/(R+T)) relative to the pKJK5 transfer efficiency in the NT control. Note that for the outgoing assay, the recipients also encoded a type IV-A3 and crRNA to avoid obscuring the interference signal by secondary pKJK5 transfer (from transconjugants to recipients) and a chromosomal Cm marker. In brief, after overnight growth of recipient and donor strains in biological triplicates and with required antibiotics, we diluted 1:100 and re-grew strains in LB + inducers and appropriate antibiotics into exponential phase (~3 h). We removed antibiotics by spinning and resuspending cultures in LB + inducers and incubated at RT for 15 min. To initiate mating cultures we spun 500 µL each, resuspended in 20 µL LB + inducers, and mixed 20 µL of donor and recipient to 40 µL mating cultures which were allowed to conjugate on LB agar plates + inducers for 3h after drying. We rescued mating drops with a loop and resuspended them in 500 µL LB prior to dilution plating on LB agar plates + inducers and appropriate antibiotics to select either donors+transconjugants, recipients+transconjugants, or transconjugants only. The outgoing assay differed only in that conjugation time was limited to 35 min and inducers were added while growing cultures to the exponential phase. It was not possible to evaluate *trfA* targeting, as pKJK5 cannot be stably maintained in the donor strain under type IV-A3 induction.

For the plasmid stability assay (**Figure 3E**) , we grew *E. coli* MG1655 encoding the type IV-A3 Cas operon and crRNAs in four biological replicates overnight in a randomized 96-well plate containing 150 µL LB with required antibiotics and 0.2 % w/v glucose to inhibit crRNA expression. To initiate the stability assay (day 0) we twice spun cultures to remove glucose and resuspended in 150 µL LB + inducers and required antibiotics. We grew cultures for 4 days with daily passaging of 1.5 µL of grown cultures into fresh medium and plating on LB agar plates + inducers and appropriate antibiotics to enumerate plasmid-carrying and plasmid-free subpopulations. To perform statistical analyses we used the detection limit of 100 CFU/ mL when we did not obtain any plasmid-carrying colonies under *trfA* targeting.

To measure population growth rates under type IV-A3 targeting and for the NT control we grew five biological replicates of the strains used above as donor $D_{IV\text{-}A3}$ in LB + required antibiotics for vector and pKJK5 selection overnight. To initiate the experiment we diluted cultures 100-fold by adding 1.5 µL to a randomized 96-well plate containing 150 µL of fresh

LB + antibiotics and inducers. Cultures grew for 20 h in a Tecan NanoQuant Infinite M200 Pro and were shaken prior to the hourly measurement.

gfp targeting in transconjugants

After the incoming pKJK5 plasmid targeting assay, we measured the green fluorescence signal of transconjugants. For each replicate of the strains targeting *gfp* in the coding (+) and template (-) strand, and the NT control, we diluted the cells in 3 mL PBS and proceeded to analyze them through flow cytometry (FACSAria Illu Becton Dickson Biosciences, San Jose, CA, USA) using a 70 µm nozzle and sheath fluid pressure of 70 lb/in2. GFP was excited by a 488 nm laser (20 mW) and detected on the fluoresceine isothiocyanate A (FITC-A) channel; bandpass filter of 530/30 nm. mCherry was excited with a 561 nm laser (50 mW) and detected on the phosphatidylethanolamine (PE)-Texas Red-A channel; bandpass filter of 610/20 nm. We set detection thresholds to 200 for forward (FSC) and side scatter (SSC) and used the BD FACSDiva software (v6.1.3) for data analyses. Briefly, we used scatterplots of particle FSC vs. SSC to delimit gates for bacterial events, thus excluding background noise. We used bivariate contour plots (FITC vs. PE-Texas Red) to gate GFP- and mCherry-positive bacterial cells. We used cell counts of 1000 to 3000 threshold events/ s, processed at flow rate 1, and recorded a total of 30,000 bacterial events for each replicate. We enumerated the following fluorescent phenotypes, i) total cells expressing mCherry (red), ii) total cells expressing *gfp* from pKJK5 and mCherry (red-and-green). We then calculated the percentage of cells that were red-and-green (transconjugants) of the total red population (recipients).

Phage targeting assay

We assessed the functionality of type IV-A3 in phage targeting through phage-spotting assays, by evaluating the replication of CRISPR-targeted phage λ-vir on bacterial lawns (GeneHogs) in comparison to the NT control. We designed crRNAs hybridizing with both DNA strands of the λ-vir genome at four selected positions, including early and late expressed genes, and an intergenic region. We chose an intergenic region between two convergently transcribed genes, for which we could not locate any putative promoters. In brief, we overexpressed the IV-A3 Cas operon under P_{tac} promoter supplemented with crRNAs (targeting and NT) expressed from P_{Bad} promoter overnight in *E. coli* GeneHogs in triplicates. We mixed 150 µL of bacterial overnight cultures with 4 mL of molten top agar (0.7 % w/v) supplemented with 10 mM MgSO4, L-arabinose (0.3 % w/v), and IPTG. We poured the mix onto LB agar plates containing MgSO4, L-arabinose, and IPTG and spotted 4 or 10 µL of 10-fold serial diluted phage lysates onto the lawn. Plates incubated at 30 °C to count PFU the next day.

Isolation of escaper phages

To isolate phages that escaped CRISPR-targeting, we spotted 20 ul of undiluted ancestor phage on the lawn of the respective targeting strain and stroked out the phage across the plate, and incubated them overnight at 30 °C. We then picked single plaques of spontaneous escapers and restreaked them on a new lawn. We repeated this single plaque isolation three times to ensure that no mixed genotypes of phages remained. We then amplified the targeted

sites via PCR and Sanger sequenced the fragments for escapers in gene B and the intergenic region. We could not get a PCR product for the R escaper and therefore extracted the total DNA from the escaper and the ancestor λ-vir phage lysate after enrichment for high phage titer (> 10^7 pfu/ mL) DNA with the DNeasy blood and tissue kit (QIAGEN), starting from the Proteinase-K treatment step to lyse the phages [103]. We prepared sequencing libraries using the Illumina NEXTERA XT Kit for tagmentation and amplification (12 cycles), following the manufacturer's instructions and purified libraries using the bead-based HighPrep™ clean-up Kit (MagBio Genomics). Paired-end sequencing was performed on an Illumina MiSeq platform using Miseq V3 chemistry (2 x 300 cycles), according to the manufacturer's protocol. We used CLC Genomics Workbench (v20.0.4) for adapter trimming and generation of de novo assemblies and annotated assembled genomes with Rapid Annotations (Subsystems Technology tool kit (RASTtk) accessed through PATRIC (v3.6.12) [104]. To determine the molecular mechanisms of escaping, we aligned escaper assemblies to the ancestral reference with snapgene (v6.0.2). With NCBI nucleotide blast (standard parameters), we identified genomic region acquired by escapers to be also located in the chromosomes of laboratory *E.coli* as (DH10B, DH5alph) from which also GeneHogs descend (e.g., NCBI: CP000948.1). We visualized phage-λ genomes with clinker v0.0.23 using standard parameters [105].

TXTL-based PAM Assay: PAM-DETECT

To identify the preferred TIM sequence for type IV-A3 target interference, we used the PAM-DETECT methodology, as described previously [37]. Briefly, we used a vector-based protospacer library with randomized TIMs. Protospacers containing a functional TIM sequence are protected from cleavage, since successful IV-A3 complex binding to the protospacer prevents plasmid cleavage in a subsequent restriction digestion step. Enrichment of TIMs is then assessed via high-throughput sequencing. We used a plasmid containing a library of five randomized nucleotides (potential TIMs) flanked by a protospacer containing a PacI restriction site, and expressed the type IV-A3 Cas (Δ*dinG*) components and crRNA from separate plasmids. The 6 µl TXTL reaction consisted of 3 nM plasmid encoding for the IV-A3 effector complex, 1 nM crRNA-encoding and PAM-library plasmid each, 0.2 nM T7 RNA polymerase, 0.5 mM IPTG, and 4.5 µL myTXTL Sigma 70 Master Mix. For the negative control we replaced the IV-A3 encoding plasmid with an equal volume of water. We incubated TXTL reactions at 29 °C for 6 h and digested at 37 °C with PacI (NEB R0547S) as instructed by the provider and added water instead of PacI for the undigested control. After PacI inactivation, we added 0.05 mg/ mL Proteinase K (Cytiva), incubated at 45 °C for 1 h and after Proteinase K inactivation extracted the remaining plasmids with standard EtOH precipitation.

For NGS library preparation we added adapters and unique dual indices in a two-step amplification process using the KAPA HiFi HotStart Library Amplification Kit (KAPA Biosystems, KK2611) and purified samples with Agencourt AMPure XP (Beckman Coulter, A63881). We used a Illumina NovaSeq 6000 (paired end, 2 × 50 bp, 2 million reads per sample) sequencer and for NGS data analysis we followed [106] and [107]. First, we normalized the read counts of

every TIM with the total number of reads and calculated the ratio of digested to undigested sample reads. The sum of ratios for a given nucleotide at a given position is then divided by the sum of the ratios of all nucleotides at that given position (resulting in 25 % in case of no enrichment/depletion). Finally, to assess the amount of library plasmid protected from restriction digestion, we performed qPCR using the SsoAdvanced Universal SYBR Green Supermix (Biorad, cat#1725271) with primers amplifying a 100 bp spanning the *Pac*I recognition site of the library plasmid and primers amplifying a 100 bp region on the T7 RNA polymerase encoding plasmid as a control. We quantified reactions with the QuantStudio Real-Time PCR System (Thermo Fisher Scientific) and an annealing temperature of 68 °C, according to manufacturers' instructions.

mCherry chromosome targeting and RNA sequencing

To shed light on the relevance of DinG for target interference through transcriptional repression, we used three type IV-A3 variants (wildtype, DinG knockout mutant Δ*dinG*, catalytically inactive DinG mutant *dinGmut*) in an assay targeting the chromosomally encoded *mCherry* or its promoter P_{lpp}. We grew four biological replicates of MG1655 for each possible combination of the IV-A3 variant and crRNA (three variants x eight crRNAs and the NT control, 27 in total) overnight with appropriate antibiotics in a 96-well plate. To initiate the experiment, we pin-replicated ~1 µL of each culture into a black (transparent bottom) 96-well plate containing 150 µL LB + appropriate antibiotics + inducers. Cultures grew for 24 hours in a Tecan NanoQuant Infinite M200 Pro. We measured OD600 and fluorescence intensity (Excitation 582 nm, Emission 620 nm) in an interval of 15 min. For each replicate and time point, we normalized the mCherry signal with the corresponding OD600 measure and selected timepoint 15 h for further analysis. To identify the best fit model explaining most of the observed variation in mCherry signal, we performed linear regression models with the three predictors IV-A3 variant, position (promoter vs. gene), and strand with interactions. Next, we performed RNAseq (Illumina NextSeq 2000) on triplicates of the WT and Δ*dinG* variants with two crRNAs (two variants x 2 crRNAs and the NT control) and extracted RNA with the mirVana isolation kit (Ambion). We used the Illumina Stranded Total RNA Prep, Ligation with Ribo-Zero Plus kit for library preparation. Starting with 200 ng total RNA per sample, we rRNA-depleted, fragmented and converted RNAs to cDNA with reverse transcriptase. The resulting cDNAs were converted to double stranded cDNAs and subjected to end-repair, A-tailing, and adapter ligation. RNAseq data were processed with the Sequana (v0.16.5) RNAseq pipeline for quality control, read mapping, and quantification of gene expression levels [108]. We visualized read coverage with pyGenomeViz (v0.4.4)[109] and computed differential expression analysis with PyDESeq2 [110] (v1.34.0, default parameters) by comparing the average of the triplicates for each sample against an average of their respecitve NT-controls. For volcano plots we used seaborn (v0.13.2) and matplotlib (v3.8.2) [111].

Bio-layer interferometry of the IV-A3 complex on double-stranded DNA

To test type IV-A3 CRISPR-Cas complex affinity to double-stranded DNA targets, we performed bio-layer interferometry experiments in size exclusion buffer corresponding to the respective analyte on an Octet K2 System (Pall ForteBio). We prepared the target dsDNA ligand by annealing oligonucleotides BTS and NTS at a ratio of 1:1.5 (5 µM BTS: 7.5 µM NTS) in size exclusion buffer by heating the annealing reaction at 95 °C for 5 min and slowly cooling it down to RT. To immobilize the dsDNA ligand on an Octet SAX 2.0 biosensors (Sartorius) we prepared 200 µL of a 25 nM dsDNA solution in a black 96-well plate and performed a loading step for 120 s followed by a washing step for 30 s. We diluted the IV-A3 complex, either with NT or targeting crRNA, from 1 µM to 25 nM in a 200 µl final volume dilution series and measured association and dissociation for 300 s and 180 s, respectively. The baseline was recorded prior and after association/dissociation for 30 s in the matching size exclusion buffer and for each measurement. A reference omitting the dsDNA from the solution was recorded to subtract reference curves from sample curves. For K_D determination the reference-subtracted binding and dissociation curves were fitted to the standard 1:1 local binding model using the Pall ForteBio analysis software.

Cell-free transcription-translation assays

To further explore the targeting activity of the distinct type IV-A3 variants observed in our *in vivo* transcriptional repression analysis, we performed a cell-free transcription-translation (TXTL) assay. We used individual plasmids encoding one of the three type IV-A3 variants (wildtype, Δ*dinG*, *dinGmut*), deGFP, and one of the *degfp*-targeting crRNAs (one on each strand of P_{T7}, four on each strand within the *degfp*; 10 in total and a NT control). Because the type IV-A3 and *degfp* are under the control of a P_{T7}, we also included a plasmid encoding the T7 RNA polymerase. To assess the targeting activity of the IV-A3 variants at distinct interference loci, we assembled the following reaction mixes using an Echo525 Liquid Handling system (Beckman Coulter, 001-10080): We added each possible combination of the IV-A3 variant and crRNA and the remaining plasmids to the myTXTL mix (Arbor Biosciences, 507025-ARB) at the following final concentrations: 2 nM each for plasmids encoding type IV-A3 and the crRNA, 1 nM of the deGFP plasmid and 0.2 nM of the T7 RNA polymerase plasmid (3 µl per reaction mix and four replicates each). To measure background fluorescence we assembled an additional mix that only contained myTXTL mix and water. We incubated these reactions at 29 °C for 16 h in a plate reader (BioTek Synergy Neo2) and measured fluorescence every 3 minutes. We plotted endpoint measurements as the RFU after subtracting the background fluorescence from each reaction.

Re-sensitizing of antibiotic-resistant strains

To investigate type IV-A3's capacity to re-sensitize bacterial strains by transcriptional repression of β-lactamases we first re-sensitized *E. coli* DH10B by targeting $bla_{CTX\text{-}M15}$ encoded on the clinical *E. coli* plasmid p1ESBL. In brief, we grew four biological replicates of targeting and NT strains, differing only in crRNA, overnight with appropriate antibiotics, and the next

day we diluted 1:100 and re-grew strains in 2 mL LB + inducers and appropriate antibiotics into exponential phase (~3 h). We spun and resuspended cultures in 80 µL LB, serially diluted, and plated them on LB agar + inducers and appropriate antibiotics to select either p1ESBL-carrying cells or $bla_{CTX\text{-}M15}$ expressing cells. To be able to enumerate plasmid-carrying cells independent of $bla_{CTX\text{-}M15}$ expression we inserted a Kan marker on p1ESBL.

Second, we re-sensitized the clinical *K. pneumoniae* 808330 (Δp1530) by targeting the chromosomal $bla_{SHV\text{-}187}$ with a combination of broth microdilution and targeting assay. We followed the 96-well plate-based MIC assay protocol from Wiegand et al. [112] but made several modifications to accommodate IVA3-interference during the assay, such as adding appropriate antibiotics for type IV-A3 and crRNA selection and inducers. Further, we substituted the Mueller-Hinton growth medium with LB. We used the same Cas operon- and mini-array setup as described for the plasmid targeting above but replaced the Amp cassette on the IV-A3 encoding pMMB67he with a Cm marker. We grew four biological replicates for strain 808330 carrying type IV-A3 and either a crRNA or the NT control overnight with appropriate antibiotics. To initiate the MIC/ targeting assay, we diluted 1:100 and re-grew strains in LB + inducers and appropriate antibiotics into exponential phase (~3 h). We measured OD600 of cultures, adjusted them to an OD600 = 0.065, and diluted 1:100 to reach a final OD600 = 0.00065 in LB + 2-fold required concentrations of inducers and the antibiotics Cm and Gm for vector selection. To assay the MICs we added 50 µL per culture to the 96-well plate containing 50µL LB per well + specific Amp concentrations (10 concentrations with two-fold reduction steps from 32-0.0625 mg/L). Further, to compare the type IV-A3 mediated MIC reduction to the one achieved by a $bla_{SHV\text{-}187}$ null-mutant we performed a MIC assay as above with 808330 (Δp1530) and the same strain with an additional Δ*SVH* mutation. Here no subculturing step prior to the MIC assay and no inducers or antibiotics additional to Amp were required. We interpreted MIC breakpoints for Amp according to EUCAST guidelines (v4.0, 2022-01-01) after 18-24 h of static growth [113]. To compare the IV-A3 mediated MIC reduction to the one achieved by the addition of the β-lactamase inhibitor clavulanic acid we performed a disk diffusion assay under targeting using Amp (10 µg) and amoxicillin-clavulanic acid (Amc; 20/10 µg). We grew four biological replicates for strain 808330 (Δp1530) carrying type IV-A3 and either a crRNA or the NT control overnight + inducers and appropriate antibiotics. We adjusted strains to OD600 = 0.02 and distributed 2 mL thereof on LB agar plates, removed excess liquid by pipetting, and placed the disks on plates after drying. After 20 h incubation, we measured the diameters of inhibition zones by hand and interpreted MIC breakpoints according to EUCAST guidelines (v13.0, 2023-01-01; [114]).

4. QUANTIFICATION AND STATISTICAL ANALYSIS

We performed all statistical analyses using R (v4.1.0). Statistical details of experiments can be found in figure legends, including the statistical test, number of replicates, and dispersion and

precision measures (e.g., mean, median, SD, SEM, confidence intervals). We plotted figures with Prism9 and used Adobe Illustrator for editing.

Supplementary Tables not included in the Supplementary Information PDF

Table S3: Type IV-A3 carrying plasmids
Table S4: Type IV-A3 targeted plasmids
Table S6: Plasmid constructs used in this study
Table S7: Oligonucleotides and DNA fragments used in this study.

References

1. Shah, S.A., Erdmann, S., Mojica, F.J.M., and Garrett, R.A. (2013). Protospacer recognition motifs: mixed identities and functional diversity. RNA Biol. *10*, 891–899. 10.4161/rna.23764.

2. Marraffini, L.A., and Sontheimer, E.J. (2010). Self versus non-self discrimination during CRISPR RNA-directed immunity. Nature *463*, 568–571. 10.1038/nature08703.

3. Makarova, K.S., Wolf, Y.I., Iranzo, J., Shmakov, S.A., Alkhnbashi, O.S., Brouns, S.J.J., Charpentier, E., Cheng, D., Haft, D.H., Horvath, P., et al. (2020). Evolutionary classification of CRISPR-Cas systems: a burst of class 2 and derived variants. Nat. Rev. Microbiol. *18*, 67–83. 10.1038/s41579-019-0299-x.

4. Liu, T.Y., and Doudna, J.A. (2020). Chemistry of Class 1 CRISPR-Cas effectors: Binding, editing, and regulation. J. Biol. Chem. *295*. 10.1074/jbc.REV120.007034.

5. Özcan, A., Pausch, P., Linden, A., Wulf, A., Schühle, K., Heider, J., Urlaub, H., Heimerl, T., Bange, G., and Randau, L. (2019). Type IV CRISPR RNA processing and effector complex formation in Aromatoleum aromaticum. Nat Microbiol *4*, 89–96. 10.1038/s41564-018-0274-8.

6. Zhou, Y., Bravo, J.P.K., Taylor, H.N., Steens, J.A., Jackson, R.N., Staals, R.H.J., and Taylor, D.W. (2021). Structure of a type IV CRISPR-Cas ribonucleoprotein complex. iScience *24*, 102201. 10.1016/j.isci.2021.102201.

7. Cui, N., Zhang, J.-T., Liu, Y., Liu, Y., Liu, X.-Y., Wang, C., Huang, H., and Jia, N. (2023). Type IV-A CRISPR-Csf complex: Assembly, dsDNA targeting, and CasDinG recruitment. Mol. Cell. 10.1016/j.molcel.2023.05.036.

8. Pinilla-Redondo, R., Mayo-Muñoz, D., Russel, J., Garrett, R.A., Randau, L., Sørensen, S.J., and Shah, S.A. (2020). Type IV CRISPR-Cas systems are highly diverse and involved in competition between plasmids. Nucleic Acids Res. *48*, 2000–2012. 10.1093/nar/gkz1197.

9. Taylor, H.N., Laderman, E., Armbrust, M., Hallmark, T., Keiser, D., Bondy-Denomy, J.,

and Jackson, R.N. (2021). Positioning Diverse Type IV Structures and Functions Within Class 1 CRISPR-Cas Systems. Front. Microbiol. *12*, 671522. 10.3389/fmicb.2021.671522.

10. Moya-Beltrán, A., Makarova, K.S., Acuña, L.G., Wolf, Y.I., Covarrubias, P.C., Shmakov, S.A., Silva, C., Tolstoy, I., Barrie Johnson, D., Koonin, E.V., et al. (2021). Evolution of Type IV CRISPR-Cas Systems: Insights from CRISPR Loci in Integrative Conjugative Elements of *Acidithiobacillia*. Preprint, 10.1089/crispr.2021.0051 10.1089/crispr.2021.0051.

11. Crowley, V.M., Catching, A., Taylor, H.N., Borges, A.L., Metcalf, J., Bondy-Denomy, J., and Jackson, R.N. (2019). A Type IV-A CRISPR-Cas System in *Pseudomonas aeruginosa* Mediates RNA-Guided Plasmid Interference *In Vivo*. Preprint, 10.1089/crispr.2019.0048 10.1089/crispr.2019.0048.

12. Newire, E., Aydin, A., Juma, S., Enne, V.I., and Roberts, A.P. (2020). Identification of a Type IV-A CRISPR-Cas System Located Exclusively on Plasmids in. Front. Microbiol. *11*, 1937. 10.3389/fmicb.2020.01937.

13. Domgaard, H., Cahoon, C., Armbrust, M.J., Redman, O., Jolley, A., Thomas, A., and Jackson, R.N. (2023). CasDinG is a 5’-3' dsDNA and RNA/DNA helicase with three accessory domains essential for type IV CRISPR immunity. Nucleic Acids Res. 10.1093/nar/gkad546.

14. Guo, X., Sanchez-Londono, M., Gomes-Filho, J.V., Hernandez-Tamayo, R., Rust, S., Immelmann, L.M., Schäfer, P., Wiegel, J., Graumann, P.L., and Randau, L. (2022). Characterization of the self-targeting Type IV CRISPR interference system in Pseudomonas oleovorans. Nat Microbiol *7*, 1870–1878. 10.1038/s41564-022-01229-2.

15. Kamruzzaman, M., and Iredell, J.R. (2019). CRISPR-Cas System in Antibiotic Resistance Plasmids in. Front. Microbiol. *10*, 2934. 10.3389/fmicb.2019.02934.

16. Pitout, J.D.D., and Laupland, K.B. (2008). Extended-spectrum β-lactamase-producing Enterobacteriaceae: an emerging public-health concern. Preprint, 10.1016/s1473-3099(08)70041-0 10.1016/s1473-3099(08)70041-0.

17. Novais, A., Comas, I., Baquero, F., Cantón, R., Coque, T.M., Moya, A., González-Candelas, F., and Galán, J.-C. (2010). Evolutionary trajectories of beta-lactamase CTX-M-1 cluster enzymes: predicting antibiotic resistance. PLoS Pathog. *6*, e1000735. 10.1371/journal.ppat.1000735.

18. Makarova, K.S., Wolf, Y.I., Alkhnbashi, O.S., Costa, F., Shah, S.A., Saunders, S.J., Barrangou, R., Brouns, S.J.J., Charpentier, E., Haft, D.H., et al. (2015). An updated evolutionary classification of CRISPR–Cas systems. Nat. Rev. Microbiol. *13*, 722. 10.1038/nrmicro3569.

19. Santiago-Frangos, A., Buyukyoruk, M., Wiegand, T., Krishna, P., and Wiedenheft, B. (2021). Distribution and phasing of sequence motifs that facilitate CRISPR adaptation. Curr. Biol. *31*, 3515–3524.e6. 10.1016/j.cub.2021.05.068.

20. Pinilla-Redondo, R., Mayo-Muñoz, D., Russel, J., Garrett, R.A., Randau, L., Sørensen, S.J., and Shah, S.A. (2020). Type IV CRISPR-Cas systems are highly diverse and involved in competition between plasmids. Nucleic Acids Res. *48*, 2000–2012. 10.1093/nar/gkz1197.

21. Yoganand, K.N.R., Sivathanu, R., Nimkar, S., and Anand, B. (2016). Asymmetric positioning of Cas1–2 complex and Integration Host Factor induced DNA bending guide the unidirectional homing of protospacer in CRISPR-Cas type I-E system. Nucleic Acids Res. *45*, 367–381. 10.1093/nar/gkw1151.

22. Nuñez, J.K., Bai, L., Harrington, L.B., Hinder, T.L., and Doudna, J.A. (2016). CRISPR Immunological Memory Requires a Host Factor for Specificity. Mol. Cell *62*, 824–833. 10.1016/j.molcel.2016.04.027.

23. Shipman, S.L., Nivala, J., Macklis, J.D., and Church, G.M. (2016). Molecular recordings by directed CRISPR spacer acquisition. Science *353*, aaf1175. 10.1126/science.aaf1175.

24. Swarts, D.C., Mosterd, C., van Passel, M.W.J., and Brouns, S.J.J. (2012). CRISPR Interference Directs Strand Specific Spacer Acquisition. Preprint, 10.1371/journal.pone.0035888 10.1371/journal.pone.0035888.

25. Yosef, I., Goren, M.G., and Qimron, U. (2012). Proteins and DNA elements essential for the CRISPR adaptation process in Escherichia coli. Preprint, 10.1093/nar/gks216 10.1093/nar/gks216.

26. Wang, J., Li, J., Zhao, H., Sheng, G., Wang, M., Yin, M., and Wang, Y. (2015). Structural and Mechanistic Basis of PAM-Dependent Spacer Acquisition in CRISPR-Cas Systems. Preprint, 10.1016/j.cell.2015.10.008 10.1016/j.cell.2015.10.008.

27. McKenzie, R.E., Almendros, C., Vink, J.N.A., and Brouns, S.J.J. (2019). Using CAPTURE to detect spacer acquisition in native CRISPR arrays. Nat. Protoc. *14*, 976–990. 10.1038/s41596-018-0123-5.

28. Díez-Villaseñor, C., Guzmán, N.M., Almendros, C., García-Martínez, J., and Mojica, F.J.M. (2013). CRISPR-spacer integration reporter plasmids reveal distinct genuine acquisition specificities among CRISPR-Cas I-E variants of Escherichia coli. RNA Biol. *10*, 792–802. 10.4161/rna.24023.

29. Pinilla-Redondo, R., Russel, J., Mayo-Muñoz, D., Shah, S.A., Garrett, R.A., Nesme, J., Madsen, J.S., Fineran, P.C., and Sørensen, S.J. (2022). CRISPR-Cas systems are widespread accessory elements across bacterial and archaeal plasmids. Preprint, 10.1093/nar/gkab859 10.1093/nar/gkab859.

30. Bahl, M.I., Hansen, L.H., Licht, T.R., and Sørensen, S.J. (2007). Conjugative Transfer Facilitates Stable Maintenance of IncP-1 Plasmid pKJK5 in *Escherichia coli* Cells Colonizing the Gastrointestinal Tract of the Germfree Rat. Preprint, 10.1128/aem.01971-06 10.1128/aem.01971-06.

31. Klümper, U., Riber, L., Dechesne, A., Sannazzarro, A., Hansen, L.H., Sørensen, S.J., and

Smets, B.F. (2015). Broad host range plasmids can invade an unexpectedly diverse fraction of a soil bacterial community. Preprint, 10.1038/ismej.2014.191 10.1038/ismej.2014.191.

32. Jaskólska, M., Adams, D.W., and Blokesch, M. (2022). Two defence systems eliminate plasmids from seventh pandemic Vibrio cholerae. Nature *604*, 323–329. 10.1038/s41586-022-04546-y.

33. Koopal, B., Potocnik, A., Mutte, S.K., Aparicio-Maldonado, C., Lindhoud, S., Vervoort, J.J.M., Brouns, S.J.J., and Swarts, D.C. (2022). Short prokaryotic Argonaute systems trigger cell death upon detection of invading DNA. Cell *185*, 1471–1486.e19. 10.1016/j.cell.2022.03.012.

34. Deveau, H., Barrangou, R., Garneau, J.E., Labonté, J., Fremaux, C., Boyaval, P., Romero, D.A., Horvath, P., and Moineau, S. (2008). Phage response to CRISPR-encoded resistance in Streptococcus thermophilus. J. Bacteriol. *190*, 1390–1400. 10.1128/JB.01412-07.

35. Sapranauskas, R., Gasiunas, G., Fremaux, C., Barrangou, R., Horvath, P., and Siksnys, V. (2011). The Streptococcus thermophilus CRISPR/Cas system provides immunity in Escherichia coli. Nucleic Acids Res. *39*, 9275–9282. 10.1093/nar/gkr606.

36. Semenova, E., Jore, M.M., Datsenko, K.A., Semenova, A., Westra, E.R., Wanner, B., van der Oost, J., Brouns, S.J.J., and Severinov, K. (2011). Interference by clustered regularly interspaced short palindromic repeat (CRISPR) RNA is governed by a seed sequence. Proc. Natl. Acad. Sci. U. S. A. *108*, 10098–10103. 10.1073/pnas.1104144108.

37. Wimmer, F., Mougiakos, I., Englert, F., and Beisel, C.L. (2022). Rapid cell-free characterization of multi-subunit CRISPR effectors and transposons. Mol. Cell *82*, 1210–1224.e6. 10.1016/j.molcel.2022.01.026.

38. Hoffer, S.M., and Tommassen, J. (2001). The phosphate-binding protein of Escherichia coli is not essential for P(i)-regulated expression of the pho regulon. J. Bacteriol. *183*, 5768–5771. 10.1128/JB.183.19.5768-5771.2001.

39. Wanner, B.L. (1996). Phosphorus assimilation and control of the phosphate regulon. Escherichia coli and Salmonella: cellular and molecular biology *1*, 1357–1381.

40. Antimicrobial Resistance Collaborators (2022). Global burden of bacterial antimicrobial resistance in 2019: a systematic analysis. Lancet *399*, 629–655. 10.1016/S0140-6736(21)02724-0.

41. Edgar, R., Friedman, N., Molshanski-Mor, S., and Qimron, U. (2012). Reversing bacterial resistance to antibiotics by phage-mediated delivery of dominant sensitive genes. Appl. Environ. Microbiol. *78*, 744–751. 10.1128/AEM.05741-11.

42. Hochvaldová, L., Panáček, D., Válková, L., Prucek, R., Kohlová, V., Večeřová, R., Kolář, M., Kvítek, L., and Panáček, A. (2022). Restoration of antibacterial activity of inactive antibiotics via combined treatment with a cyanographene/Ag nanohybrid. Sci. Rep. *12*,

5222. 10.1038/s41598-022-09294-7.

43. Bikard, D., and Barrangou, R. (2017). Using CRISPR-Cas systems as antimicrobials. Curr. Opin. Microbiol. *37*, 155–160. 10.1016/j.mib.2017.08.005.

44. Benz, F., and Hall, A.R. (2023). Host-specific plasmid evolution explains the variable spread of clinical antibiotic-resistance plasmids. Proc. Natl. Acad. Sci. U. S. A. *120*, e2212147120. 10.1073/pnas.2212147120.

45. Benz, F., Huisman, J.S., Bakkeren, E., Herter, J.A., Stadler, T., Ackermann, M., Diard, M., Egli, A., Hall, A.R., Hardt, W.-D., et al. (2021). Plasmid- and strain-specific factors drive variation in ESBL-plasmid spread in vitro and in vivo. ISME J. *15*, 862–878. 10.1038/s41396-020-00819-4.

46. Bernheim, A., Bikard, D., Touchon, M., and Rocha, E.P.C. (2020). Atypical organizations and epistatic interactions of CRISPRs and cas clusters in genomes and their mobile genetic elements. Nucleic Acids Res. *48*, 748–760. 10.1093/nar/gkz1091.

47. Peters, J.E., Makarova, K.S., Shmakov, S., and Koonin, E.V. (2017). Recruitment of CRISPR-Cas systems by Tn7-like transposons. Proc. Natl. Acad. Sci. U. S. A. *114*, E7358–E7366. 10.1073/pnas.1709035114.

48. Al-Shayeb, B., Skopintsev, P., Soczek, K.M., Stahl, E.C., Li, Z., Groover, E., Smock, D., Eggers, A.R., Pausch, P., Cress, B.F., et al. (2022). Diverse virus-encoded CRISPR-Cas systems include streamlined genome editors. Cell *185*, 4574–4586.e16. 10.1016/j.cell.2022.10.020.

49. Weissman, J.L., Stoltzfus, A., Westra, E.R., and Johnson, P.L.F. (2020). Avoidance of Self during CRISPR Immunization. Preprint, 10.1016/j.tim.2020.02.005 10.1016/j.tim.2020.02.005.

50. Klompe, S.E., Vo, P.L.H., Halpin-Healy, T.S., and Sternberg, S.H. (2019). Transposon-encoded CRISPR-Cas systems direct RNA-guided DNA integration. Nature *571*, 219–225. 10.1038/s41586-019-1323-z.

51. Strecker, J., Ladha, A., Gardner, Z., Schmid-Burgk, J.L., Makarova, K.S., Koonin, E.V., and Zhang, F. (2019). RNA-guided DNA insertion with CRISPR-associated transposases. Science *365*, 48–53. 10.1126/science.aax9181.

52. Rybarski, J.R., Hu, K., Hill, A.M., Wilke, C.O., and Finkelstein, I.J. (2021). Metagenomic discovery of CRISPR-associated transposons. Proc. Natl. Acad. Sci. U. S. A. *118*. 10.1073/pnas.2112279118.

53. Al-Shayeb, B., Sachdeva, R., Chen, L.-X., Ward, F., Munk, P., Devoto, A., Castelle, C.J., Olm, M.R., Bouma-Gregson, K., Amano, Y., et al. (2020). Clades of huge phages from across Earth's ecosystems. Nature *578*, 425–431. 10.1038/s41586-020-2007-4.

54. Wu, W.Y., Mohanraju, P., Liao, C., Adiego-Pérez, B., Creutzburg, S.C.A., Makarova, K.S., Keessen, K., Lindeboom, T.A., Khan, T.S., Prinsen, S., et al. (2022). The miniature

CRISPR-Cas12m effector binds DNA to block transcription. Mol. Cell *82*, 4487–4502.e7. 10.1016/j.molcel.2022.11.003.

55. Tesson, F., and Bernheim, A. (2023). Synergy and regulation of antiphage systems: toward the existence of a bacterial immune system? Curr. Opin. Microbiol. *71*, 102238. 10.1016/j.mib.2022.102238.

56. Rocha, E.P.C., and Bikard, D. (2022). Microbial defenses against mobile genetic elements and viruses: Who defends whom from what? PLoS Biol. *20*, e3001514. 10.1371/journal.pbio.3001514.

57. Little, J.W., and Mount, D.W. (1982). The SOS regulatory system of Escherichia coli. Cell *29*, 11–22. 10.1016/0092-8674(82)90085-x.

58. Janion, C. (2001). Some aspects of the SOS response system--a critical survey. Acta Biochim. Pol. *48*, 599–610.

59. Malone, L.M., Hampton, H.G., Morgan, X.C., and Fineran, P.C. (2022). Type I CRISPR-Cas provides robust immunity but incomplete attenuation of phage-induced cellular stress. Nucleic Acids Res. *50*, 160–174. 10.1093/nar/gkab1210.

60. Wegrzyn, G., and Wegrzyn, A. (2002). Stress responses and replication of plasmids in bacterial cells. Microb. Cell Fact. *1*, 2. 10.1186/1475-2859-1-2.

61. Huang, C.J., Adler, B.A., and Doudna, J.A. (2022). A naturally DNase-free CRISPR-Cas12c enzyme silences gene expression. Mol. Cell *82*, 2148–2160.e4. 10.1016/j.molcel.2022.04.020.

62. Quinones-Olvera, N., Owen, S.V., McCully, L.M., Marin, M.G., Rand, E.A., Fan, A.C., Martins Dosumu, O.J., Paul, K., Sanchez Castaño, C.E., Petherbridge, R., et al. (2023). Diverse and abundant viruses exploit conjugative plasmids. bioRxiv. 10.1101/2023.03.19.532758.

63. Qi, L.S., Larson, M.H., Gilbert, L.A., Doudna, J.A., Weissman, J.S., Arkin, A.P., and Lim, W.A. (2013). Repurposing CRISPR as an RNA-guided platform for sequence-specific control of gene expression. Cell *152*, 1173–1183. 10.1016/j.cell.2013.02.022.

64. Bikard, D., Jiang, W., Samai, P., Hochschild, A., Zhang, F., and Marraffini, L.A. (2013). Programmable repression and activation of bacterial gene expression using an engineered CRISPR-Cas system. Nucleic Acids Res. *41*, 7429–7437. 10.1093/nar/gkt520.

65. Kim, S.K., Kim, H., Ahn, W.-C., Park, K.-H., Woo, E.-J., Lee, D.-H., and Lee, S.-G. (2017). Efficient Transcriptional Gene Repression by Type V-A CRISPR-Cpf1 from Eubacterium eligens. ACS Synth. Biol. *6*, 1273–1282. 10.1021/acssynbio.6b00368.

66. Zhang, X., Wang, J., Cheng, Q., Zheng, X., Zhao, G., and Wang, J. (2017). Multiplex gene regulation by CRISPR-ddCpf1. Cell Discov *3*, 17018. 10.1038/celldisc.2017.18.

67. Luo, M.L., Mullis, A.S., Leenay, R.T., and Beisel, C.L. (2015). Repurposing endogenous

type I CRISPR-Cas systems for programmable gene repression. Nucleic Acids Res. *43*, 674–681. 10.1093/nar/gku971.

68. Cassini, A., Högberg, L.D., Plachouras, D., Quattrocchi, A., Hoxha, A., Simonsen, G.S., Colomb-Cotinat, M., Kretzschmar, M.E., Devleesschauwer, B., Cecchini, M., et al. (2019). Attributable deaths and disability-adjusted life-years caused by infections with antibiotic-resistant bacteria in the EU and the European Economic Area in 2015: a population-level modelling analysis. Lancet Infect. Dis. *19*, 56–66. 10.1016/S1473-3099(18)30605-4.

69. Bikard, D., Euler, C.W., Jiang, W., Nussenzweig, P.M., Goldberg, G.W., Duportet, X., Fischetti, V.A., and Marraffini, L.A. (2014). Exploiting CRISPR-Cas nucleases to produce sequence-specific antimicrobials. Nat. Biotechnol. *32*, 1146–1150. 10.1038/nbt.3043.

70. Uribe, R.V., Rathmer, C., Jahn, L.J., Ellabaan, M.M.H., Li, S.S., and Sommer, M.O.A. (2021). Bacterial resistance to CRISPR-Cas antimicrobials. Sci. Rep. *11*, 17267. 10.1038/s41598-021-96735-4.

71. Kroll, J., Klinter, S., Schneider, C., Voss, I., and Steinbüchel, A. (2010). Plasmid addiction systems: perspectives and applications in biotechnology. Microb. Biotechnol. *3*, 634–657. 10.1111/j.1751-7915.2010.00170.x.

72. Citorik, R.J., Mimee, M., and Lu, T.K. (2014). Sequence-specific antimicrobials using efficiently delivered RNA-guided nucleases. Nat. Biotechnol. *32*, 1141–1145. 10.1038/nbt.3011.

73. Wick, R.R., Judd, L.M., Gorrie, C.L., and Holt, K.E. (2017). Unicycler: Resolving bacterial genome assemblies from short and long sequencing reads. PLoS Comput. Biol. *13*, e1005595. 10.1371/journal.pcbi.1005595.

74. Russel, J., Pinilla-Redondo, R., Mayo-Muñoz, D., Shah, S.A., and Sørensen, S.J. (2020). CRISPRCasTyper: Automated Identification, Annotation, and Classification of CRISPR-Cas Loci. CRISPR J *3*, 462–469. 10.1089/crispr.2020.0059.

75. Carattoli, A., Zankari, E., García-Fernández, A., Voldby, L.M., Lund, O., Villa, L., Møller, A.F., and Hasman, H. (2014). In silico detection and typing of plasmids using PlasmidFinder and plasmid multilocus sequence typing. Antimicrob. Agents Chemother. *58*. 10.1128/AAC.02412-14.

76. Robertson, J., and Nash, J.H.E. (2018). MOB-suite: software tools for clustering, reconstruction and typing of plasmids from draft assemblies. Microbial Genomics *4*, e000206. 10.1099/mgen.0.000206.

77. Alcock, B.P., Huynh, W., Chalil, R., Smith, K.W., Raphenya, A.R., Wlodarski, M.A., Edalatmand, A., Petkau, A., Syed, S.A., Tsang, K.K., et al. (2023). CARD 2023: expanded curation, support for machine learning, and resistome prediction at the Comprehensive Antibiotic Resistance Database. Nucleic Acids Res. *51*. 10.1093/nar/gkac920.

78. Huisman, J.S., Benz, F., Duxbury, S.J.N., de Visser, J.A.G.M., Hall, A.R., Fischer, E.A.J.,

and Bonhoeffer, S. (2022). Estimating plasmid conjugation rates: A new computational tool and a critical comparison of methods. Plasmid *121*, 102627. 10.1016/j.plasmid.2022.102627.

79. Alva, V., Nam, S.-Z., Söding, J., and Lupas, A.N. (2016). The MPI bioinformatics Toolkit as an integrative platform for advanced protein sequence and structure analysis. Nucleic Acids Res. *44*, W410–W415. 10.1093/nar/gkw348.

80. Katoh, K., and Standley, D.M. (2013). MAFFT multiple sequence alignment software version 7: improvements in performance and usability. Mol. Biol. Evol. *30*, 772–780. 10.1093/molbev/mst010.

81. Guindon, S., Dufayard, J.-F., Lefort, V., Anisimova, M., Hordijk, W., and Gascuel, O. (2010). New Algorithms and Methods to Estimate Maximum-Likelihood Phylogenies: Assessing the Performance of PhyML 3.0. Syst. Biol. *59*, 307–321. 10.1093/sysbio/syq010.

82. Letunic, I., and Bork, P. (2021). Interactive Tree Of Life (iTOL) v5: an online tool for phylogenetic tree display and annotation. Nucleic Acids Res. *49*, W293–W296. 10.1093/nar/gkab301.

83. Blackwell, G.A., Hunt, M., Malone, K.M., Lima, L., Horesh, G., Alako, B.T.F., Thomson, N.R., and Iqbal, Z. (2021). Exploring bacterial diversity via a curated and searchable snapshot of archived DNA sequences. PLoS Biol. *19*, e3001421. 10.1371/journal.pbio.3001421.

84. Schmartz, G.P., Hartung, A., Hirsch, P., Kern, F., Fehlmann, T., Müller, R., and Keller, A. (2022). PLSDB: advancing a comprehensive database of bacterial plasmids. Nucleic Acids Res. *50*, D273–D278. 10.1093/nar/gkab1111.

85. Li, W., and Godzik, A. (2006). Cd-hit: a fast program for clustering and comparing large sets of protein or nucleotide sequences. Bioinformatics *22*, 1658–1659. 10.1093/bioinformatics/btl158.

86. Camacho C., Coulouris G., Avagyan V., Ma N., Papadopoulos J., Bealer K., Madden T.L. BLAST+: architecture and applications. BMC Bioinformatics *10*. 10.1186/1471-2105-10-421.

87. Feldgarden, M., Brover, V., Gonzalez-Escalona, N., Frye, J.G., Haendiges, J., Haft, D.H., Hoffmann, M., Pettengill, J.B., Prasad, A.B., Tillman, G.E., et al. (2021). AMRFinderPlus and the Reference Gene Catalog facilitate examination of the genomic links among antimicrobial resistance, stress response, and virulence. Sci. Rep. *11*, 12728. 10.1038/s41598-021-91456-0.

88. Pfeifer, E., Bonnin, R.A., and Rocha, E.P.C. (2022). Phage-Plasmids Spread Antibiotic Resistance Genes through Infection and Lysogenic Conversion. MBio *13*, e0185122. 10.1128/mbio.01851-22.

89. Cury, J., Abby, S.S., Doppelt-Azeroual, O., Néron, B., and Rocha, E.P.C. (2020).

Identifying Conjugative Plasmids and Integrative Conjugative Elements with CONJscan. Methods Mol. Biol. *2075*, 265–283. 10.1007/978-1-4939-9877-7_19.

90. Ares-Arroyo, M., Coluzzi, C., and Rocha, E.P.C. (2023). Origins of transfer establish networks of functional dependencies for plasmid transfer by conjugation. Nucleic Acids Res. *51*, 3001–3016. 10.1093/nar/gkac1079.

91. Wickham, H. ggplot2 (Springer International Publishing) 10.1007/978-3-319-24277-4.

92. Conway, J.R., Lex, A., and Gehlenborg, N. (2017). UpSetR: an R package for the visualization of intersecting sets and their properties. Bioinformatics *33*, 2938–2940. 10.1093/bioinformatics/btx364.

93. Wilke, C. (2022). ggridges: Ridgeline Plots in “ggplot2”. R package version 0.5.4,. https://wilkelab.org/ggridges/.

94. Wingett, S.W., and Andrews, S. (2018). FastQ Screen: A tool for multi-genome mapping and quality control. F1000Res. *7*, 1338. 10.12688/f1000research.15931.2.

95. Martin, M. (2011). Cutadapt removes adapter sequences from high-throughput sequencing reads. EMBnet.journal *17*, 10–12. 10.14806/ej.17.1.200.

96. Kim, D., Langmead, B., and Salzberg, S.L. (2015). HISAT: a fast spliced aligner with low memory requirements. Nat. Methods *12*, 357–360. 10.1038/nmeth.3317.

97. Thrash, A., Arick, M., and Peterson, D.G. (2018). Quack: A quality assurance tool for high throughput sequence data. Anal. Biochem. *548*. 10.1016/j.ab.2018.01.028.

98. Mortazavi, A., Williams, B.A., McCue, K., Schaeffer, L., and Wold, B. (2008). Mapping and quantifying mammalian transcriptomes by RNA-Seq. Nat. Methods *5*. 10.1038/nmeth.1226.

99. Wickham, H. (2009). ggplot2: Elegant Graphics for Data Analysis (Springer Science & Business Media).

100. Datsenko, K.A., and Wanner, B.L. (2000). One-step inactivation of chromosomal genes in Escherichia coli K-12 using PCR products. Proc. Natl. Acad. Sci. U. S. A. *97*, 6640–6645. 10.1073/pnas.120163297.

101. Bolger, A.M., Lohse, M., and Usadel, B. (2014). Trimmomatic: a flexible trimmer for Illumina sequence data. Bioinformatics *30*, 2114–2120. 10.1093/bioinformatics/btu170.

102. Zhang, J., Kobert, K., Flouri, T., and Stamatakis, A. (2014). PEAR: a fast and accurate Illumina Paired-End reAd mergeR. Bioinformatics *30*, 614–620. 10.1093/bioinformatics/btt593.

103. Jakočiūnė, D., and Moodley, A. (2018). A Rapid Bacteriophage DNA Extraction Method. Methods Protoc *1*. 10.3390/mps1030027.

104. Brettin, T., Davis, J.J., Disz, T., Edwards, R.A., Gerdes, S., Olsen, G.J., Olson, R., Overbeek, R., Parrello, B., Pusch, G.D., et al. (2015). RASTtk: a modular and extensible implementation of the RAST algorithm for building custom annotation pipelines and annotating batches of genomes. Sci. Rep. *5*, 8365. 10.1038/srep08365.

105. Gilchrist, C.L.M., and Chooi, Y.-H. (2021). clinker & clustermap.js: automatic generation of gene cluster comparison figures. Bioinformatics *37*, 2473–2475. 10.1093/bioinformatics/btab007.

106. Leenay, R.T., Maksimchuk, K.R., Slotkowski, R.A., Agrawal, R.N., Gomaa, A.A., Briner, A.E., Barrangou, R., and Beisel, C.L. (2016). Identifying and Visualizing Functional PAM Diversity across CRISPR-Cas Systems. Mol. Cell *62*, 137–147. 10.1016/j.molcel.2016.02.031.

107. Ondov, B.D., Bergman, N.H., and Phillippy, A.M. (2011). Interactive metagenomic visualization in a Web browser. BMC Bioinformatics *12*, 1–10. 10.1186/1471-2105-12-385.

108. Cokelaer, T., Desvillechabrol, D., Legendre, R., and Cardon, M. (2017). "Sequana": a Set of Snakemake NGS pipelines. Journal of Open Source Software *2*, 352. 10.21105/joss.00352.

109. GitHub - moshi4/pyGenomeViz: A genome visualization python package for comparative genomics GitHub. https://github.com/moshi4/pyGenomeViz.

110. Muzellec, B., Teleńczuk, M., Cabeli, V., and Andreux, M. (2023). PyDESeq2: a python package for bulk RNA-seq differential expression analysis. Bioinformatics *39*. 10.1093/bioinformatics/btad547.

111. Waskom, M.L. (2021). seaborn: statistical data visualization. Journal of Open Source Software *6*, 3021. 10.21105/joss.03021.

112. Wiegand, I., Hilpert, K., and Hancock, R.E. (2008). Agar and broth dilution methods to determine the minimal inhibitory concentration (MIC) of antimicrobial substances. Nat. Protoc. *3*. 10.1038/nprot.2007.521.

113. ESCMID-European Society of Clinical Microbiology, and Diseases, I. eucast: MIC determination. https://www.eucast.org/ast_of_bacteria/mic_determination.

114. ESCMID-European Society of Clinical Microbiology, and Diseases, I. eucast: Clinical breakpoints and dosing of antibiotics. https://www.eucast.org/clinical_breakpoints.

115. Huynh, B.-T., Passet, V., Rakotondrasoa, A., Diallo, T., Kerleguer, A., Hennart, M., De Lauzanne, A., Herindrainy, P., Seck, A., Bercion, R., et al. (2020). Klebsiella pneumoniae carriage in low-income countries: antimicrobial resistance, genomic diversity and risk factors. Gut Microbes. 10.1080/19490976.2020.1748257.

116. Diard, M., and Hardt, W.-D. (2017). Basic Processes in -Host Interactions: Within-Host Evolution and the Transmission of the Virulent Genotype. Microbiol Spectr *5*.

10.1128/microbiolspec.MTBP-0012-2016.

117. GitHub - moshi4/pyGenomeViz: A genome visualization python package for comparative genomics GitHub. https://github.com/moshi4/pyGenomeViz.